William M. Gelbart Avinoam Ben-Shaul
Didier Roux Editors

Micelles, Membranes, Microemulsions, and Monolayers

With 220 Illustrations

Springer-Verlag
New York Berlin Heidelberg London Paris
Tokyo Hong Kong Barcelona Budapest

12

Structures and Phase Transitions in Langmuir Monolayers

David Andelman[1]
Francoise Brochard[2]
Charles Knobler[3]
Francis Rondelez[4]

12.1 Introduction

Throughout the previous chapters, attention has been focused on the wide variety of structures and phase behaviors characterizing the self-assembly of amphiphilic molecules in aqueous solution (Chapters 1 to 6) and in oil/water mixtures (Chapters 6 to 11). In all cases the organization of amphiphilic (surfactant) molecules has involved one or more *three*-dimensional aggregates, *i.e.*, globular or cylindrical micelles, vesicles or undulating bilayers, and droplets or bicontinuous phases of microemulsions. As a consequence, elastic (curvature) free energy has played a crucial role in determining the relative stabilities of competing geometries, and the associated phase transitions have been naturally compared and contrasted with those familiar from the usual fluids, liquid crystals, and solids *in bulk*.

In the present, concluding, chapter we turn to an important class of *two*-dimensional (2D) phenomena, in particular those arising in the study of adsorbed amphiphilic monolayers on a liquid subphase. It has long been known that many amphiphilic molecules form monomolecular layers at the interface between water and air. If the amphiphile is only very slightly soluble in the bulk, it can be treated as a separate surface phase; such an

[1]Department of Physics, Tel Aviv University, Ramat Aviv, Tel Aviv, 69978 Israel
[2]Laboratoire de Physico-Chimie des Surfaces et Interfaces (CNRS-URA 1379), Institut Curie—Section de Physique et Chimie, 11 rue Pierre et Marie Curie, Paris 75231, Cedex 05, France
[3]Department of Chemistry and Biochemistry, University of California Los Angeles, Los Angeles, California 90024, USA
[4]Same as footnote 2

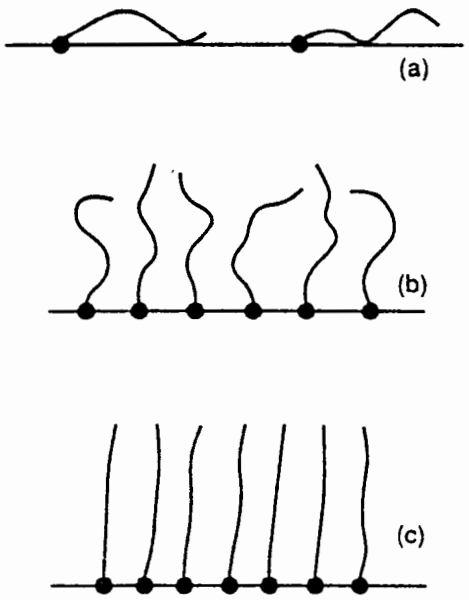

FIGURE 12.1. Schematic representation of the microscopic structure of a monolayer in different states. The dots represent the hydrophilic head and the wavy lines the hydrophobic tails of the amphiphiles. (a) Gas: the molecules are widely separated and the tails are in contact with the water surface; (b) Intermediate density: the tails are upright but disordered; (c) Condensed state: the tails are almost entirely in *trans* conformations and closely packed.

insoluble film is called a Langmuir monolayer. Langmuir monolayers can be formed when there is the right balance between the solubility of the hydrophilic head group of the amphiphile and the hydrophobic nature of its tail. For substances like fatty acids, this balance can be achieved for chain lengths that fall between 12 and 30 carbons. Insoluble monolayers of phospholipids and simple esters are also easily formed.

The microscopic nature of a Langmuir monolayer is suggested by the cartoons shown in Fig. 12.1. The head groups are immersed in the water surface and the tails remain out of the water. At low density the tails are likely to be disordered and will have conformations that bring them in contact with the water surface. (Recall that hydrophobicity does not imply a repulsive interaction between the tail and the water surface.) If the monolayer density is increased by compression at constant temperature, the chains begin to interact and are more likely to be found above the water surface. As the packing becomes tighter the chains are increasingly in the *trans* conformation (see Sec. 1.3.3). At the highest densities the chains and head groups are completely ordered and the packing is similar to that found in the three-dimensional solid.

The complex interplay between energetic and entropic factors in monolayers is similar to that found in other amphiphilic systems. What is new

here is the possibility of continuously changing the area per amphiphile, the constraint brought about by the pinning of the head groups to the surface and the interaction of both the chains and the head groups with the subphase. A further complication arises because the amphiphiles are necessarily dipolar. Thus, when the density is sufficiently high to orient the chains, the molecular dipoles are aligned and repel each other; if the chains are tilted with respect to the surface there will be both in-plane and out-of-plane dipolar interactions.

While the structures of Langmuir monolayers are far from being completely understood, there have been many recent experimental and theoretical advances, which are the subject of this chapter. We will begin (Sec. 12.2.1) with a review of results from what can be called classical studies, work that is not necessarily old but which has been carried out with the techniques that were developed by the early workers in the field. A variety of new experimental methods has led to a revitalization of monolayer research; these will be described briefly in Sec. 12.2.2. A critique of the current experimental situation then follows in Sec. 12.2.3. In Sec. 12.3 we discuss first (12.3.1) the equilibrium theories of successive fluid-fluid phase transitions and chain conformational statistics, and then the driving forces for spatially modulated states in Langmuir monolayers (12.3.2-12.3.3). *Dynamical* features of these systems are treated in Sec. 12.4, followed by a concluding discussion in 12.5.

12.2 The Experimental Situation

12.2.1 Classical Studies

Langmuir monolayers can be prepared by depositing a small amount of a solution of an amphiphile in a volatile solvent onto a clean water surface; the monolayer forms spontaneously as the solvent spreads and evaporates. The area available to the monolayer is controlled by a barrier that can be slid across the surface, as shown in Fig. 12.2. Detailed descriptions of the experimental methods outlined below are found in the books by Gaines [1] and Adamson [2].

The thermodynamic state of the monolayer can be described by an equation of state $\Pi = \Pi(a, T)$ where Π is a two-dimensional pressure, T is the temperature, and a is the area per molecule. The surface pressure is defined as the difference between γ_o, the surface tension of pure water and γ the surface tension in the presence of the monolayer (see Chap. 10):

$$\Pi = \gamma_o - \gamma \tag{12.1}$$

In writing $\Pi(a, T)$ we have assumed that the properties of the subphase have been held constant. The properties of the monolayer, however, may be sensitive to the pH or ionic strength of the subphase or to the presence in the bulk of specific solutes such as divalent ions.

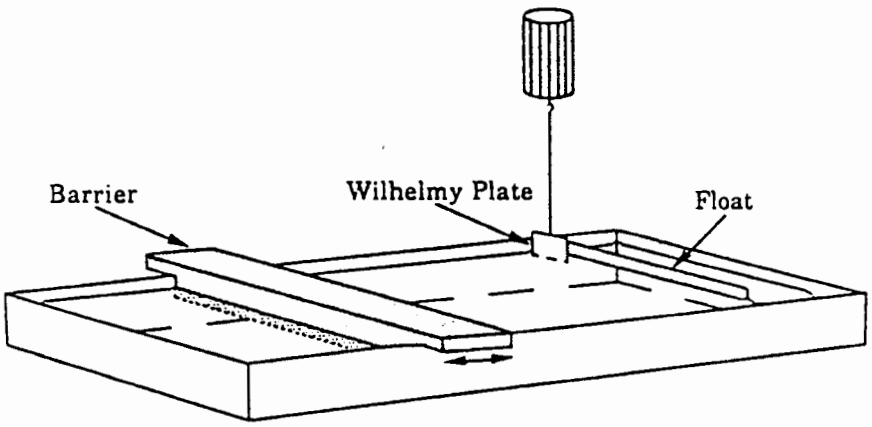

FIGURE 12.2. Schematic diagram of a Langmuir trough. The trough is typically constructed of a material such as Teflon that is not wetted by water; the water surface therefore rises above the edge. Monolayers can be compressed by sliding the barrier across the surface. The pressure can be determined by measuring the force on a plate (Wilhelmy plate) that passes through the surface or on a barrier that separates the monolayer-covered surface from pure water.

The most common measurement performed on Langmuir monolayers is the determination of surface pressure–area isotherms, and much of the information concerning the phase behavior of monolayers has been deduced from such studies. The schematic isotherm shown in Fig. 12.3 is typical of those observed for many pure amphiphiles. As in the case of $P - V$ isotherms, first-order transitions should be marked by horizontal portions of the isotherm and second-order transitions by changes in slope. Thus, for example, the long plateau at low pressure arises from a first-order transition between a gaseous phase and a fluid phase.

Unfortunately, the interpretation of isotherms is often not so straightforward because the slopes in first-order transition regions are rarely truly horizontal. Further, transitions between condensed phases may be accompanied by only very small changes in density so that the isotherms exhibit kinks rather than plateaus. Phase diagrams have therefore been established only by combining isotherm studies with measurements of other properties.

The character of a phase can be assessed, for example, from measurements of the surface potential ΔV, which can be related to p_z, the component of the dipole moment density of the film perpendicular to the interface, by the relation

$$\Delta V = p_z/\varepsilon^* \tag{12.2}$$

where ε^* is the local dielectric constant seen by the dipoles. The observed potentials can be compared to those predicted for models of the monolayer in which the charge distribution along the amphiphile is estimated from

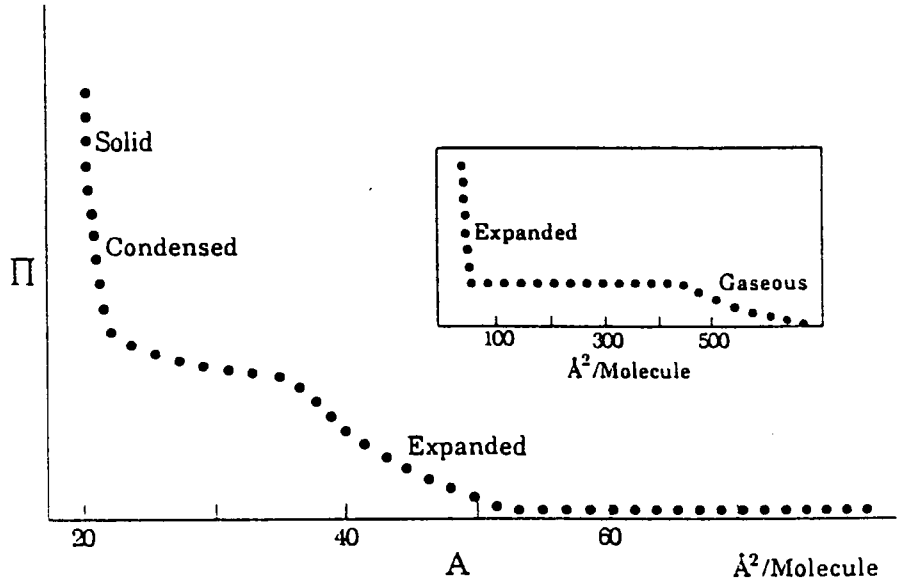

FIGURE 12.3. Schematic $\Pi - a$ isotherm. The long plateau corresponds to the G-LE two-phase region. The short plateau, which corresponds to the LE-LC two-phase region, is horizontal only in measurements made with extremely pure materials; it is not observed in all monolayers. The isotherm is simplified; other more subtle features may also be observed in precise measurements.

its chemical structure and for which a conformation and orientation are assumed. The interpretation of such data is not without its subtleties, but useful information can often be obtained without recourse to a model. For example, temporal variations in the surface potential indicate a first-order phase transition and the coexistence of domains of different densities within the monolayer. The fluctuations arise when domains move into or out of the region beneath the measuring electrode.

Although the location of phase boundaries and the characterization of the phases by these classical methods have often been ambiguous, there has been general (but not unanimous) agreement about the existence of at least four monolayer phases that are associated with easily detectable features in isotherms: (1) Gas (G); (2) Liquid [usually called *liquid expanded* (LE)]; (3) Solid (S); and (4) Another condensed phase that intrudes between the LE and S phases and is usually called *liquid condensed* (LC). However, other features such as kinks and changes in slope are often observed in isotherms. If each of these is taken as evidence of a phase transition, many more phases must exist.

Rather complex phase diagrams, similar to the general $\Pi - T$ diagram shown in Fig. 12.4, were constructed by Stenhagen [3,4] and Lundquist [5,6] from their detailed $\Pi - a$ measurements on fatty acids and fatty esters, respectively. Their proposals were looked upon with skepticism because of the difficulties in determining subtle features in isotherms, but recent

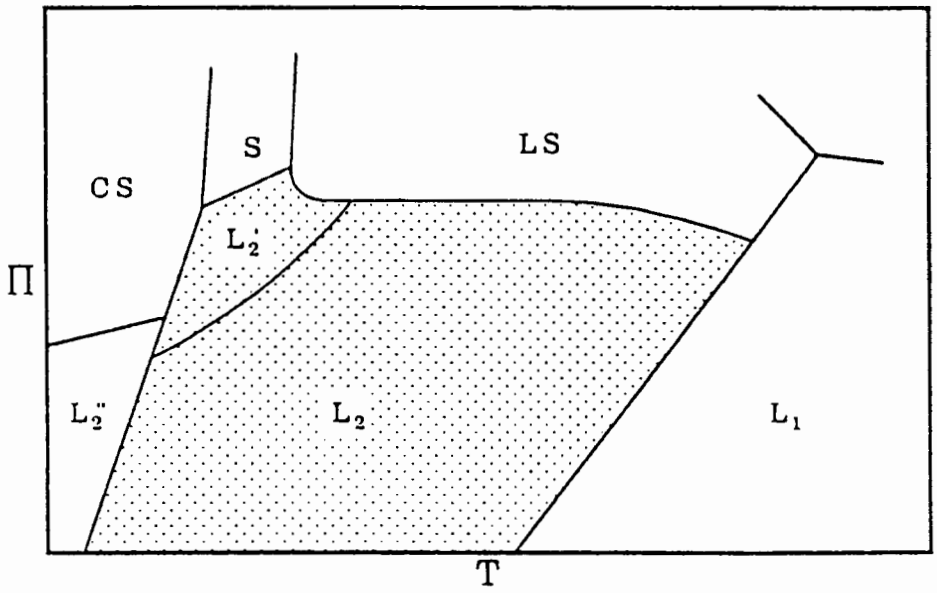

FIGURE 12.4. Generalized $\Pi - T$ diagram. The diagram is similar to the ones proposed by Stenhagen [3,4] and is applicable to long-chain fatty acids, esters, and alcohols. Adapted from Bibo *et al* [55].

studies by a variety of new methods have shown that many condensed phases *do* exist and that the Stenhagen and Lundquist diagrams are largely correct – see Section 12.2.3.1 below.

Much of the current research on Langmuir monolayers is directed toward determining the structures of the phases, understanding the relations between them and explaining them in terms of the molecular properties of the amphiphiles. These questions can be addressed only with great difficulty by the classical methods for studying monolayers, and a variety of new techniques have therefore been employed. We will give a brief overview of these methods in the next section; a more detailed discussion can be found in other reviews [7,8].

12.2.2 New Experimental Methods

12.2.2.1 Fluorescence microscopy

The textures of Langmuir monolayers can be observed directly with the technique of fluorescence microscopy [9-11]. The amphiphile is mixed with a small amount (< 1 *mol*%) of a fluorescent probe, which is usually itself an amphiphile to which a chromophore has been chemically bonded. The monolayer is then prepared in a trough mounted on the stage of an optical microscope. The fluorescence is excited by illuminating the surface, generally from above, with light from a mercury arc or laser. The fluorescence image is then observed through the microscope; it is weak and is therefore

usually detected with a high-sensitivity television camera and viewed on a monitor or recorded on videotape for subsequent analysis.

Figure 12.5 shows fluorescence images for monolayers of pentadecanoic acid at various stages of compression along a 25°C isotherm [12]. Midway through the G-LE plateau region, one sees dark circular bubbles of the G phase surrounded by the bright LE phase. The contrast between the phases is caused by the difference in density and also by a quenching of the fluorescence in the G phase. The proportion of light and dark regions varies with density according to the "lever rule"; at one phase boundary the image is completely dark while at the other it is completely bright.

The image remains uniformly bright as the monolayer is compressed through the LE one-phase region. Dark circular domains of the LC phase appear at the LE-LC phase boundary; the LC phase appears dark because the probe is only slightly soluble in it. As the compression proceeds in this two-phase region, the image becomes increasingly black as LE phase is converted into LC phase. If the probe concentration is sufficiently low, one can observe the complete transformation to the LC phase.

In some cases information about the tilt of amphiphile tails can be gained from fluorescence microscopy [13]. By tilt we mean a preferred orientation (direction) for the projection of the molecular axes onto the subphase surface. In such experiments a polarized laser that strikes the monolayer obliquely is used for excitation. If the electric field of the laser is properly oriented with respect to the surface normal, there can be a contrast in fluorescence between regions of differing tilt. This method has recently been used to examine domain structures in ester monolayers [14].

12.2.2.2 X-ray and neutron reflectometry and scattering

Monolayers have been investigated both by x-ray [15] and neutron [16] scattering. X-ray reflectivity measurements can be performed with conventional sources, but all of the X-ray diffraction studies have been carried out with synchrotron sources, which have very high intensity. The ease with which the neutron scattering cross section can be varied by isotopic substitution makes experiments with the much lower intensity neutron sources nevertheless attractive [17].

The information that can be obtained from scattering measurements on monolayers depends on the scattering vector Q, which is fixed by the source and detector geometry. Reflectance measurements are carried out by keeping Q perpendicular to the surface. In this geometry the variations of the scattered intensity with wave vector provide information about the density profile of the monolayer normal to the surface. Such measurements are analyzed by comparing the experimental scattering with that predicted for slab models in which the monolayer is envisioned as a series of layers of different thicknesses and scattering density, each slab representing some portion of the surface (subphase, head, tail). The scattering densities are computed

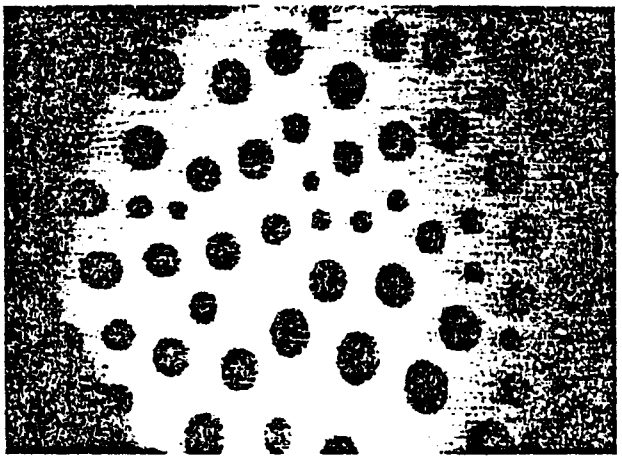

(a)

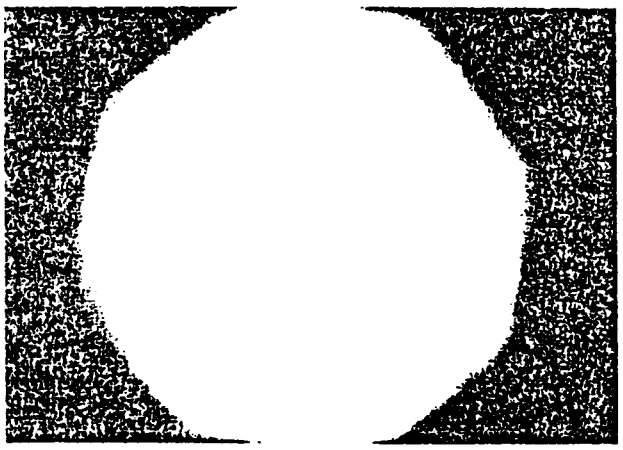

(b)

FIGURE 12.5. Fluorescence microscope images of a pentadecanoic acid monolayer at various stages of compression along a 25°C isotherm. (a) G-LE coexistence at 61 $Å^2$/molecule; (b) LE phase at 37 $Å^2$ /molecule.

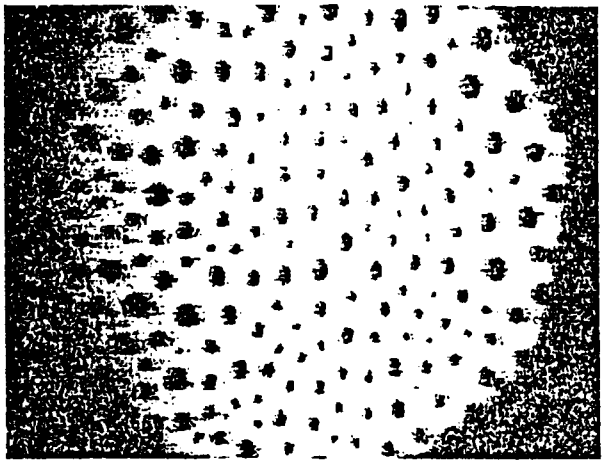

(c)

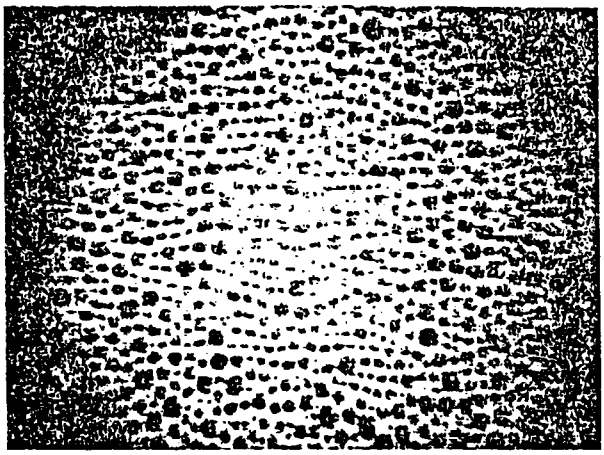

(d)

FIGURE 12.5. (c) LE-LC coexistence at 27Å^2/molecule; (d) LE-LC coexistence at 24Å^2/molecule.

from the molecular structures, and the thicknesses are determined by fitting the data; parameters are also included to account for surface roughness.

In the in-plane geometry, one studies the scattering parallel to the surface plane as a function of the scattering angle. This diffraction pattern is characteristic of the structure of the monolayer projected onto this plane. Because the source generally illuminates about 1 cm^2 of the surface, an area that includes many monolayer domains, the resulting pattern is powder averaged and does not show the isolated peaks characteristic of single crystals. The spacing of the diffraction planes can be calculated from the

peak positions and the range of the translational correlations can be obtained from the peak widths. Measurements of the intensity of a Bragg reflection along a surface normal, "rod scans" [18], allow direct information to be obtained about chain tilt.

These diffraction experiments are always difficult to perform because of the small scattered intensities Even with the most powerful synchrotron sources, they require long-time exposures and care has to be exercised to maintain the monolayer chemical integrity under the X-ray irradiation and not to lose molecules by dissolution in the subphase. This explains why such experiments have generally been confined to the longest fatty acids (with eighteen carbon atoms or more) or phospholipids and at high surface densities. One notable exception is the study of fluorinated fatty acids with only twelve carbon atoms, and over a range of surface densities between 30 and 400Å^2 per molecule [19]. Advantage is taken of the larger scattering power of fluorine atoms compared to hydrogen, and of the rod-like conformation of the CF_2 chains.

12.2.2.3 Spectroscopic measurements

The monolayer represents an extremely small part of the entire experimental system: monolayer + substrate, so the most promising spectroscopic methods are those which somehow discriminate against bulk phases. One such technique is based on the nonlinear process of optical second harmonic generation (SHG). When an intense laser beam interacts with a medium that is not centrosymmetric, a second harmonic of the laser frequency is produced. Interfaces between two uniform media lack inversion symmetry and can therefore be used to generate second harmonics.

If the signal comes mainly from the monolayer, the nonlinear susceptibility that is responsible for the generation of the second harmonic is proportional to the product of the monolayer surface density and nonlinear polarizability averaged over the distribution of molecular orientations [20,21]. In general, the relation between the molecular orientation and the signal is complex, but with some simplifying assumptions it is possible to determine the average value of the polar angle between the surface normal and the axis of the part of the molecule whose nonlinear susceptibility is involved. In most cases this SHG-active part is localized in the *head group*, so one must be careful about inferring from these analyses the average orientation of the molecular *tails*; this point is especially problematic when the chain is flexible (as at larger areas in the LE phase).

In sum-frequency generation (SFG) spectroscopy [22], another nonlinear technique that can provide surface-specific information, light from a laser operating in the visible region is mixed on the surface with light from a laser operating in the infrared. When the frequency of the infrared laser matches an absorption frequency of the monolayer, there is a resonance enhancement of the signal. The technique therefore allows the infrared spectrum of the

monolayer to be investigated. Direct measurement of the infrared spectrum of monolayers by external reflection infrared spectroscopy has also been carried out [23].

12.2.2.4 Langmuir-Blodgett films

A monolayer can be transferred to the surface of a solid substrate if the slide is passed from the water to the air side of an interface covered by the monolayer. If the solid is now passed back to the water side, a second layer is transferred. This process can be repeated to build up multilayer structures on solid supports; such structures are called Langmuir-Blodgett (LB) films. Much of the research on LB films has focused on the properties of multilayers, but monolayers have also been examined.

Many experiments that cannot be carried out on Langmuir monolayers can be performed with relative ease on LB monolayers. For example, the structures of LB films can be investigated by electron diffraction [24], a technique that can examine small domains and therefore does not produce a powder-averaged diffraction pattern. LB films can also be examined by electron microscopy [25] and by scanning tunneling [26] and atomic force microscopy [27]. The relevance of such experiments to Langmuir monolayers depends on the extent to which the properties of the monolayer are altered in the transfer process. This is not always clear, so comparisons between Langmuir monolayers and the LB films derived from them must be made with some caution.

12.2.2.5 Other methods

Several other techniques have been applied in a few instances to monolayer studies. Relaxation processes in monolayers, for example, can be studied by flow [1] or oscillating-disk viscometry [28, 29]; more detailed information on the 2D visco-elastic properties can be obtained by light scattering from thermally excited surface waves [30]. Ellipsometric measurements, which can be interpreted in terms of film thickness, have long been employed [1]; the development of modern instrumentation has sparked a renewed interest in such studies [31]. A recent development [32,33] is Brewster-angle microscopy, which allows imaging of a monolayer without the addition of fluorescent probes.

12.2.3 The Current Situation

The results of the classical studies – mainly isotherm and surface potential measurements, but also including investigations of quantities as diverse as the viscosity and the rates of chemical reactions in a monolayer – can be combined with those obtained with the newer techniques to provide a current consensus about monolayer phase diagrams and the microscopic nature of the phases.

12.2.3.1 Phase diagrams

Although there are certainly differences in detail, the number and type of general monolayer phases – G, LE, LC, and S – and their relative locations on a $\Pi - T$ diagram appear to be much the same for many phospholipids, fatty acids, alcohols, and esters. One can envision a generalized phase diagram that is displaced in some regular fashion as the nature of the head groups and tails are altered. There is, for example, a long-established rule of thumb that the addition of one CH_2 group to the tail of a fatty acid displaces the phase boundaries to higher temperature by 8–10°C. The molecular areas at which phase transitions occur must also depend in a regular fashion on the cross-sectional area and flexibility of the tails. For example, recent experiments on myristic, pentadecanoic, and palmitic acid have shown that the part of the phase diagrams corresponding to the LE-LC transition can be exactly superimposed by shifting the temperature scale by 11.6°C [34]. Condensed phases for amphiphiles such as the phospholipids, that have two chains per head group, can be expected to differ in detail from those for single-chain molecules because of packing constraints produced by the mismatch between the chain and head-group areas and differences in symmetry.

At high areas and low pressures all monolayers exist as gaseous phases. In many cases, there is a transition to the LE phase on compression; it is clear from a large variety of experiments - isotherms, surface potential, fluorescence microscopy, scattering from surface waves - that this transition is first order. It also appears likely that it ends at a critical point.

Highly precise measurements of G-LE isotherms for pentadecanoic acid [35] appeared to show the existence of a G-LE critical point at 26.27°C, but more recent isotherm studies [36] on the same system lead to the conclusion that the critical temperature must be in excess of 40°C. Fluorescence experiments [12] are in accord with these latter studies but do not explain why the two very careful isotherm experiments should give such disparate results. A detailed analysis of the first isotherms had shown that the critical point had mean-field character rather than the non-classical Ising-like behavior that might have been expected. The subsequent experiments call this conclusion into question and the character of the critical point remains unknown [37].

When the LE phase is compressed, a transition to a more condensed phase, the LC phase, is often observed. With few exceptions [38,39], horizontal isotherms are not observed in the LE-LC transition region and there has therefore been considerable debate about the order of the transition. Fluorescence measurements clearly show the presence of two phases throughout the transition region and the changes in the relative amounts of the phases follow the lever rule, so the first-order character of the transition is no longer in doubt.

The LE-LC transition is not found at low temperatures and the point at which it disappears, the LE-LC-G triple point, can be located from isotherm studies. The triple point can also be determined by fluorescence microscopy and in recent measurements on pentadecanoic acid [12] there was excellent agreement between the two methods. At temperatures below the triple point, there is a direct transition from the G phase to the LC phase without an intervening LE phase. This is the case, for example, for isotherms of stearic acid at room temperature, which lack the coexistence region associated with the LE-LC phase transition.

The existence of transitions between other condensed phases can be inferred from isotherm measurements [3,4,40] and has now been confirmed by diffraction measurements. X-ray studies of phospholipids [15,41-43], fatty acids [15,44-47] and a long-chain alcohol [48,49] have shown that there are a number of condensed monolayer phases. For example, five distinct phases that correspond to features in isotherms were distinguishable by in-plane scattering measurements on docosanoic acid. Following the notion established by Harkins and Stenhagen [3,4], they can be identified as the S, CS, LS, L_2, and L_2' phases shown in Fig. 12.4, and will be discussed in Sec. 12.2.3.2 immediately below.

The fluorescence technique can also provide evidence of such transitions. When monolayers of methyl esters are formed in the LE-LC two-phase region at high temperatures, the LC domains are circular. If the monolayer is then cooled, the domains undergo a transition to a hexagonal shape at a well-defined temperature [14,50]. The shape transition is reversible and does not depend on the nature or concentration of the fluorescent probe. One can associate the domain shape change with a transition between two LC phases, a high-temperature phase that is isotropic, and a low-temperature phase that is anisotropic. The transition temperatures correlate well with those of the $LS - L_2'$ phase transitions deduced from Lundquist's isotherms [5].

Similarly, two different patterns have been observed for LC domains of long-chain fatty acids in the LE-LC two-phase region, depending on temperature [34]. At low temperatures the domains are circular whereas highly ramified, fractal-like structures are observed at high temperatures. The shape transition is extremely sharp and occurs within less than 0.1°C, evidence that the LE phase can transform into two different LC phases. The transition temperatures correlate well with the phase diagram proposed by Bibo and Peterson [40] on the basis of surface pressure isotherms. It should be emphasized however that in these cases, the LC domains are always circular at equilibrium, and the shape transitions are associated with nonequilibrium morphologies that occur under rapid compression or changes in temperature. The relaxation rate towards the equilibrium, circular, domain shape gives information about the monolayer viscosity. It appears that the viscosity of the high-temperature phase is three orders of magnitude larger than that of the low-temperature LC phase.

A transition, presumably LE-S, has also been observed by fluorescence microscopy in a highly-compressed monolayer of stearic acid, labeled with NBD (4-nitrobenz-2-oxa-1,3-diazole) which is itself a probe molecule [51]. In this case the solid domains take the form of extremely long and narrow needles. This peculiar shape has recently been explained on the basis of the dipole-dipole interactions associated with the conjugated rings of the NBD chromophore [52].

12.2.3.2 Structures of monolayer phases

The very low density of the gas phase makes it very difficult to study by any of the techniques that provide information about microscopic structure. The low surface pressures at which the gas phase is stable also present problems for the classical studies, because even very low levels of impurities can significantly affect the measurements. Isotherms at large areas per molecule can be fit to equations of state appropriate to a two-dimensional van der Waals gas. One finds then that the effective compact area per chain is considerably larger than that for a vertical chain, which is consistent with a structure in which the chains are disordered – both conformationally and orientationally – to a large extent. Such a structure makes sense on both energetic and entropic grounds.

The classical picture of the LE phase as one in which the chains begin to be raised off the surface is consistent with that obtained from the more recent studies. SHG measurements on pentadecanoic acid [18] have been shown to be sensitive to the orientation of the head group; if the chains are assumed to be rigid, then the measurements can be interpreted in terms of change in chain orientation. At 25°C and a molecular area of 45Å^2, the polar angle with respect to the surface normal is nearly 90° in the LE phase (*i.e.*, the chains are on average nearly horizontal) but it falls sharply upon compression to about 45° at the LE-LC phase boundary (molecular area of 32Å^2). The angle then changes linearly with area, as it would if there were a mixture of phases with different tilt angles, and reaches 30° at the end of the transition region. Similar results are found along other isotherms between 20 and 30°C, and it appears that the 45° angle at the start of the LE-LC transition is independent of temperature.

Sum-frequency spectra have also been measured [22] in the LE phase of pentadecanoic acid. A strong CH_2 asymmetric stretch signal at 2850cm^{-1} and a broad background in the range 2880 – 2930cm^{-1} that is also attributable to CH_2 stretches are observed. The intensities of these features increase when the monolayer is expanded further. If the chains were straight, there would be near inversion symmetry along them, and the CH_2 modes would not be observed. Thus the presence of the modes and the increase in intensity is indicative of an increase in *gauche* conformations in the tail as the area increases.

Fourier transform infrared spectroscopy (FTIR) studies of the LE phase in dipalmitoyl phosphatidylcholine (DPPC) [53] also provide information

about changes in the *gauche/trans* ratio. For DPPC monolayers at a molecular area of 100Å^2, the CH_2 stretching frequency corresponds to that found in bulk suspensions; it decreases linearly with decreasing area, and in the LC phase reaches a value comparable to that in pure bulk DPPC in which the chains are all *trans*.

X-ray reflectivity measurements have been performed [15] on dimyristoyl phosphatidic acid (DMPA) at an area of 87 ± 7Å^2, which is in the LE one-phase region. The thickness in the LE phase is markedly less than in the LC phase. If one takes the chains in the LC phase to be vertical, then the thickness observed for the LE phase corresponds to a tilt of 50° if the chains were all *trans*.

The results of the early diffraction measurements on monolayers were difficult to correlate because they were performed on several different substances in different thermodynamic states. Some features of the structures could be generalized, however. The widths of the diffraction peaks showed that the positional correlation length in all but one of the phases (called the compact solid phase) was short, at most 100 lattice spacings. All of the structures can be seen to arise from an hexagonal packing of the head groups but may have a lower symmetry because of chain tilt or chain packing in phases in which the chains do not rotate. The chains are essentially fully *trans* in the condensed phase. On the other hand, electron diffraction experiments [24,25,54] have shown that there can be extremely long-range lattice orientational order since the diffraction spots are observed not to rotate in space as the sample is translated over several microns.

Peterson and his coworkers [46,55] have shown that the structures of the acids, esters, and alcohols can be understood in terms of four order parameters that have been used to characterize smectic liquid crystalline phases, and that each of the condensed monolayer phases can be seen as the 2-D analog of a known smectic phase [55]. These parameters are (1) Positional order (PO); (2) Bond or lattice orientational order (BO); (3) Tilt order (TO), which is the order of the molecular tilt azimuth with respect to the local orientational order; (4) Herringbone order (HO), which is the staggered ordering of the planes of the all-trans hydrocarbon chains. A distinction is made between quasi-long-range order, in which the order decays according to a power law and short-range order, in which the order falls off exponentially with distance. The order parameters for each of the smectic phases are shown in Table 12.1, and the correspondence between the monolayer and smectic phases is also given in Table 12.1.

Detailed isotherm measurements [55] on acid + ester mixtures suggest the existence of four "LC" phases, that is four phases that can coexist with the LE phase. All four of the phases (LS, L_2^*, L_1', and L_2) are hexatic phases in which there is quasi-long-range orientational order. They differ in their tilt order: the chains in the LS phase are untilted, so there is no TO; in the L_2^* phase the chains are tilted towards their next-nearest neighbor (NNN) in

TABLE 12.1. SMECTIC PHASES AND THEIR PROPOSED RELATION TO MONOLAYER PHASES. The smectic phases are characterized by four order parameters: PO (In-plane positional correlations); TO (Molecular tilt azimuth); BO (Bond or lattice orientation); and HO (Herringbone order or broken axial symmetry). The column T-O indicates the direction of the tilt azimuth with respect to the bond orientation: NN (toward nearest neighbors); NNN (toward next-nearest neighbors). The corresponding monolayer phases are specified in the Harkins-Stenhagen nomenclature. There are in addition a gaseous phase and the CS phase, which is taken to be a true 2-D crystal.

SMECTIC TYPE	PO	TO	BO	T-B	HO	MONOLAYER PHASE
A	S	S	S		S	LE
BC	L	S	L		S	
BH	S	S	L		S	LS
C	S	L	S		S	
E	L	S	L		L	S
F	S	L	L	NNN	S	L_2'
G	L	L	L	NNN	S	
H	L	L	L	NNN	L	S'
I	S	L	L	NN	S	L_2
J	L	L	L	NN	S	
K	L	L	L	NN	L	L_2''
L	S	L	L	I	S	L_1'

the locally hexagonal structure; the tilt is towards nearest neighbors (NN) in the L_2 phase; and toward a direction intermediate between NN and NNN in L_1'. There is no HO because the chains rotate freely and therefore have effective cylindrical symmetry.

All of these phases have been identified in diffraction studies. Proof of the existence of tilt order can be seen in the polarized fluorescence microscopy experiments by Xiu *et al* [14]. They showed that distinct regions of uniform tilt appeared in LC domains on cooling out of the LS phase. In some cases the tilt regions in a domain are organized into "star defects", Fig. 12.6, which had been observed in freely suspended films of hexatic liquid crystals [56]. It is evident from the figure that some of these defects are chiral, even though the ester and the probe are not. This identifies the phase as L_1', because it is the only intrinsically chiral hexatic (Table 12.1).

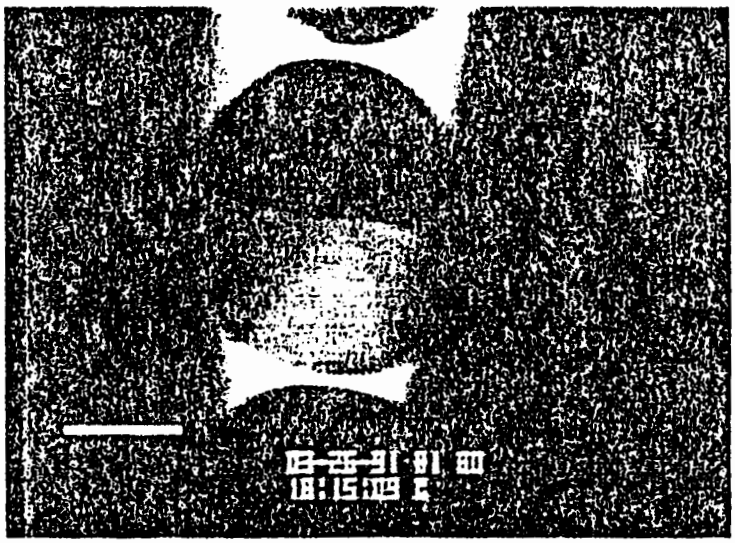

FIGURE 12.6. Regions of uniform tilt in an LC domain of methyl eicosanoate at 20°C. The tilt regions are evident only if the exciting radiation is polarized.

12.3 Equilibrium Theories of Monolayers

12.3.1 Fluid-Fluid Phase Transitions and Chain Statistics

At very low surface densities, when the average area per molecule a is much larger than the cross sectional area of an isolated chain, a^*, an adsorbed amphiphilic monolayer behaves as a 2D gas. Recall from Chap. 1 — Sec. 1.3.3 in particular — that a^* is the projected area of a single chain whose head is constrained at a planar interface: $a^* \simeq 40\text{Å}^2$, say, for a 12-carbon alkyl tail. For $a \geq a^*$, then, a molecule in a monolayer is still free to "express" its conformational entropy without interference from neighbors. As discussed above, a clear first-order phase transition from the gas-phase (G) to a "liquid-expanded" (LE) phase is observed upon compression of the monolayer. The area per molecule on the gas-phase side of the transition is typically $a_G \approx 300 - 1500\text{Å}^2$ whereas on the LE side it is on the order of the cross-sectional area of an *isolated* chain, *i.e.*, $a_{LE} \simeq a^*$. The second phase transition, to the "liquid-condensed" (LC) state, observed upon further compression of the monolayer, is associated with a change in area from $a_{LE} \approx 30 - 40\text{Å}^2$ to $a_{LC} \approx 22 - 25\text{Å}^2$, which is just barely larger than the cross-sectional area of a fully stretched (all-trans) chain. The main difficulty in understanding the LE-LC transition is in identifying the structure of the two phases and the driving force (order parameter) of the transition between them. Some insight can be gained by considering an analogy with liquid crystalline systems.

Rod-like (or disk-like) molecules forming liquid crystalline systems undergo an isotropic-nematic, (I→N) transition in three dimensions without the need for attractive forces between particles [57]. Here a discontinuous onset of orientational order (alignment) appears spontaneously upon compression (or cooling, in the case where attractive interactions are also operative [58]). Based on this analogy one naively expects that the LE→LC transition will be analogous to the I→N transition in liquid crystals. However, if the adsorbed molecules are treated as rigid rods that interact through their excluded volumes, it can be shown [59] that the increase in orientational order upon compression is continuous. Subsequently, it was shown by Chen *et al* [60] that because of the lower symmetry of the monolayer compared to that of a bulk liquid, a system of rigid, adsorbed rods will not undergo a first-order fluid-fluid phase transition upon compression unless there are attractive forces acting between the particles. For this latter case they showed that only a single transition occurs, essentially a gas→liquid condensation at which there is also (in addition to the jump in density) a discontinuous change from weak to stronger long-range orientational ordering.

This situation contrasts with the experimental situation described above in which the amphiphilic monolayer is observed to undergo two, successive transitions between fluid phases, *i.e.*, G→LE followed by LE→LC. As discussed in the preceding section, the LC "fluid" appears to be a hexatic phase, but we shall suppress this fact for the moment. Since amphiphilic molecules are not rigid rods, the existence of two fluid-fluid transitions can be related to the chain flexibility [60], *i.e.*, to the conformational degrees of freedom of the amphiphilic chains. In fact, it is possible for attracting *rigid* rods to undergo successive G→LE and LE→LC changes of state, but only if the particles are adsorbed at the surface with an energy that depends on orientation so as to favor "lying down" vs. "standing up" [61]. Nevertheless, a number of mean-field, renormalization group, and computer simulation studies of Ising- and Potts-like models have been carried out [62,63] in which the presence of a second phase transition is explicitly attributed to coupling of chain stretching and grafting density. To amplify this basic idea we briefly and qualitatively consider the various contributions to the free energy of the monolayer.

The four major terms in the free energy of the monolayer are:

$$F = F_{\mathrm{tr}} + F_{\mathrm{conf}} + F_{\mathrm{att}} + F_{\mathrm{head}} \tag{12.3}$$

The $F_{\mathrm{tr}} = -TS_{\mathrm{tr}}$ corresponds to the translational entropy of the molecules. To a first approximation, in the gas phase, F_{tr} per molecule is

$$F_{\mathrm{tr}}/N \approx -k_B T \log(a - a^*) \tag{12.4}$$

where N is the number of molecules in the monolayer and $a - a^*$ represents

the "free area" per chain, giving rise to a lateral pressure

$$\Pi_{tr} = -\frac{1}{N}\partial F_{tr}/\partial a = k_B T/(a - a^*) \tag{12.5}$$

as in the familiar van der Waals equation. The second term, F_{conf}, represents the conformational free energy of the chain, which involves an energetic contribution associated with the internal energy of the chain (the energy of a "gauche" bond is of order $k_B T$) and an entropic term reflecting the large number Ω of possible chain conformations:

$$S_{conf} = N k_B \log \Omega \tag{12.6}$$

For an isolated chain ($a \geq a^*$) of $(n+2)$ C–C bonds, Ω can be estimated simply from, say, a 3-state rotational-isomer-state model: $\Omega \approx 3^n$. Of course as a decreases (below a^*) so does Ω, reaching $\Omega = 1$ if all chains are in the all-trans state. F_{att} denotes the attractive interaction energy between the chains. (Recall that the repulsive interactions are included in principle in F_{tr}). Like F_{tr} and F_{conf}, F_{att} is also a function of a. In the gas phase, *i.e.*, when $a > a^*$, it has a van der Waals-like form:

$$\frac{F_{att}}{N} = \frac{E_{att}}{N} \approx \frac{-\text{const.}}{a} \tag{12.7}$$

where the constant prefactor is temperature dependent. Finally, the last contribution to F includes the interaction between the head groups. This latter term, F_{head}, plays a central role in determining the character of the highly compressed (LC and, even more so, solid) phases. The contribution of the polar heads is discussed in the following section. Here, in discussing the G→LE and LE→LC transitions, we assume, as a first approximation, that F_{head} is a constant, independent of the thermodynamic variables a and T.

Now recall that in the G→LE transition both coexisting phases correspond to areas per molecule a that are larger than the area of an isolated, single, chain a^*. Thus, the conformational degrees of freedom are not severely perturbed in this transition, *i.e.*, $F_{conf}(\text{G}) \approx F_{conf}(\text{LE})$. In other words, G→LE involves mainly an interplay between F_{tr} and F_{att}. Of course these are the same two terms responsible for ordinary gas-liquid transitions. Indeed, in our case, we should not expect a different behavior as long as the conformational degrees of freedom are not affected. (The chains "look the same" on both sides of the transitions.) Here the chain "blobs" play the role of the inflexible molecules in an ordinary G-L transition: the "order parameter" of the transitions is still the surface density, $1/a$.

Once the LE phase is formed and $a \simeq a^*$, very little translational freedom is left to the chains, a condition that does not change much as the monolayer is further compressed to $a < a^*$. On the other hand this compression involves important, and opposing, changes in F_{conf} and F_{att}. Recall that

— by definition of a^* — as soon as a decreases below a^* the chains begin to feel significant constraints on their conformational degrees of freedom. Regarding F_{conf}, it can be shown (based on simple scaling arguments [64]) that to a first approximation the (dominant) entropy term varies with a according to $S_{\text{conf}} \sim 1/a^2$. It can also be argued that as the chains are compressed and thus stretched the average attraction energy between different chains varies as

$$F_{\text{att}} = E_{\text{att}} \sim -d/a^k \tag{12.8}$$

where $k \geq 1$ and d is a (nearly temperature-independent) constant. The basic idea here is that chains can attract each other more strongly ($k > 1$) when they are stretched, since a greater number of monomer-monomer contacts becomes possible between them. (An actual estimate of k requires information on the density profile of the chains, as discussed below.) Accordingly, it is the interplay between the loss of conformational entropy and the gain in chain monomer contacts that induces the LE→LC transition. In this sense, the LE→LC transition is similar to the so-called "liquid crystalline-gel" transition in bilayers [65] in which the two major contributions to the free energy are also the chain segment density and the chain conformational free energy.

In the theory of Shin *et al* [66], the decomposition described above is treated systematically via introduction of explicit models for the flexible chains. In particular, they consider the free energy of the adsorbed amphiphilic monolayer to be a sum of the following contributions: mixing entropy associated with amphiphilic molecules and solvent (water) in the surface layer; interaction energy involving chain monomers on the surface, *i.e.*, adsorption on the surface and attraction to other monomers (both intra- and inter-chain) which are adsorbed; and interaction energy involving the chain segments that lie above the water surface. The first contribution is taken to have the Flory–Huggins form [67], and the second to be described by a random mixing (Bragg–Williams [68]) approximation. For the third contribution, the interaction between the chain segments that lie above the surface, three very different models for chain behavior are considered, referring specifically to the extreme cases of flexible chains and stiff chains. The key result is that conclusions concerning the nature of fluid-fluid phase transitions are largely independent of details about the inter-chain monomer-monomer interactions above the surface or about the adsorption energy.

Even in the dilute gas phase, part of the hydrocarbon chain is found to be above the surface, consistent with the demands of conformational and/or orientational entropy. The G-LE transition is then seen to be a condensation of the in-surface portions of the chains, with essentially no change in the overall chain configuration. The LE-LC transition, on the other hand, involves a significant increase in the fraction of chain lying above the surface and — concomitantly — a condensation of the chain segments above the

surface. Consistent with this interpretation, it is found that the in-surface monomer-monomer attraction produces the G-LE transition, but has essentially no effect in the LE-LC region. Conversely, a sufficiently negative above-surface interaction energy is necessary for the LE-LC transition to occur, whereas it is largely irrelevant to G-LE.

Cantor and McIlroy [69] had earlier found a similar set of conclusions, but from a somewhat different theoretical description. They consider flexible chains attached via their head groups to a planar interface and characterize each chain configuration by the profile of volume it occupies perpendicular to this plane. The lateral-excluded-area profile of each conformation is approximated as an average over all pairs of conformations, and the monolayer entropy is determined by assuming ideal, two-dimensional, mixing of the chains with "solvent" (air or oil) and with each other. The amphiphilic chains are also characterized by the position and orientation of their surface area available for nearest-neighbor contact, for purposes of calculating interaction energies. These latter are reduced to two parameters, one related to the chain-"solvent" interfacial tension (*i.e.*, either chain/air or chain/oil) and the other to oil-water interfacial tensions. A modified cubic lattice model of chain conformations is then used to calculate $\Pi - a$ isotherms: for strong enough attractions between monomers it is found that two, successive, fluid-fluid phase transitions occur, both being characterized by a critical point. Taking the limit of rigid chains, only a single G→LE transition appears, consistent with an earlier conclusion [60]. This last point has been recently verified experimentally [70]. If the monolayer is formed with perfluorinated fatty acids, which are rigid, only a single G → LC phase transition is observed at all experimentally accessible temperatures. However a second, LE → LC phase transition is restored if a flexible spacer of four methylene units is introduced between the rigid chain and the head group.

Detailed insight into orientational and conformational structure can be obtained in principle from computer simulation of amphiphilic monolayers. Extensive molecular dynamics computations of this kind have been carried out [71,72]. However, in this work the special structure of the subphase (water!) has been neglected and the simulations have been performed in the small area per molecule limit of the adsorbed monolayer. The methylene groups of the aliphatic tails interact with each other and with the surface via a Lennard-Jones potential. Valence bond bending (*e.g.*, deviations from tetrahedral C–C–C angles) and dihedral torsional (*i.e.*, *trans-gauche* energy difference) potentials are used to provide the correct conformational statistics for the chains. Consistent with the "rod-scan" diffraction measurements, the angle of tilt is found to vary sharply upon change in the area per molecule but quantitative agreement with experiment is still lacking.

More importantly, the machine computations do not yet provide any indication of a phase transition between "expanded" and "condensed" state

of the adsorbed liquid. In order to treat properly the subtle effects associated with this transformation it will almost certainly be necessary to confront directly the molecular structure of the water "subphase". One expects in particular that the preferred orientations and interactions between head groups will depend sensitively on the "reconstruction" of water near its surface. While simulations of the free surface of water have been carried out by several groups [73], no consensus has emerged for describing the local structure at the interface. Furthermore, the presence of an adsorbed monolayer of amphiphiles will surely disrupt the surface to a significant degree: much work remains to be done before a microscopic understanding of this situation can be achieved. In general, because of the delicate interplay of competing forces involved, one must expect a wide range of different behaviors as one looks from one system to the next. For example, some will show a molecular tilt in the LC phase, whereas others will not; others will "skip" directly from the LE phase to the high-pressure solid (*i.e.*, without passing first through the LC phase) at room temperature.

12.3.2 Pattern Formation and Domain Shapes

A striking phenomenon observed in monolayers is the formation of patterns, some quite complex, which can be observed directly by fluorescence microscopy. The patterns range from foam structures that are seen at low densities corresponding to the G-LE coexistence region, to fractal structures, dendrites, hexagonal arrays, and spirals that have been observed at higher densities. What is the origin of these patterns and what controls their shapes? Are these patterns equilibrium structures or do they appear only when a system is driven out of equilibrium, for example either by temperature or pressure quenches? Can one learn anything about the microscopic structure of monolayer phases from the study of these patterns?

McConnell, Möhwald and their coworkers [74,75] have made extensive studies of pattern formation in phospholipid monolayers of DPPC. These experiments have been interpreted independently by several groups [76-80] in terms of a model in which the equilibrium shape of an isolated domain is determined by the competition between electrostatic forces and line tension. In the condensed phases to which this model is applied, the amphiphiles have similar orientations and there is a repulsive, long-range, dipole-dipole interaction.

The free energy of a domain can be written as $F = \lambda L + F_{el}$ where λ is the line tension, L is the perimeter of the domain, and F_{el} is the electrostatic energy resulting from the interaction of the molecular dipoles of the amphiphiles. Surface potential measurements demonstrate that there is a marked difference in the dipole density μ_z between the LE and LC phases. Miller and Möhwald [81] have also demonstrated this in elegant experiments in which individual domains are manipulated by electrodes. As a result of these opposing contributions, the free energy of a domain

depends on both its shape and on its size. The model therefore predicts that transitions between one shape and another can occur at certain critical sizes, in accord with experiments in which circular domains undergo shape transitions as they grow [82].

In the expression for the free energy of a domain written above, the line tension is assumed to be isotropic. The formation of hexagonal LC domains in methyl esters, spiral structures in DPPC monolayers, chiral patterns in monolayers prepared from pure DPPC enantiomers and dendrites in chiral fatty amino acids demonstrate that this is not the case. This anisotropy can result from in-plane components of the molecular dipole, related either to chain tilt and/or anisotropy of the head group.

The key parameter in pattern formation is the ratio λ/μ_z^2. The addition of the "line-active" agent cholesterol to a monolayer reduces λ and leads to more extended structures. Changes of λ with temperature can also induce shape transitions. In the binary system DPPC + cholesterol, there is coexistence between two phases, one DPPC-rich, the other cholesterol-rich, that ends at an upper critical solution temperature [83,84]. As the critical point is approached from below, the line tension between the phases decreases and there is a sharp transition from circular to noncircular droplets [84].

Fluorescence micrographs show that large areas in monolayers are often organized into "superlattices" of regions with different density. These may be hexagonal arrays or lamellar structures. Some of these spatial patterns, such as foams, are clearly nonequilibrium structures because they evolve with time, but other patterns do not change during the period of typical experiments, times of a day or more.

One can take the point of view that these superlattices represent ordered regions of two distinct phases (e.g., LE and LC, or LE and G) that are metastable. The slow evolution to larger domains might be attributed to the lack of gravity as a driving force and the small differences in curvature free energy between relatively large but different size domains. From another point of view these superlattices can be taken to be one-phase regions in which there is a spatially modulated density. Just such an interpretation has been applied to the patterned phases observed in magnetic bubble domains and ferrofluids [85-87]. The morphology of superlattices in such iron garnet films are remarkably similar to those observed in monolayers.

Can one decide between these two pictures: metastable ordered two-phase regions or modulated one-phase regions? Helm and Möhwald [88] found that when dilauryl phosphatidylethanolamine (DLPE) was compressed into the LE-LC coexistence region the shapes of the domains were an equilibrium property but the size and number of the domains (and hence the superlattice spacing) depended on the nucleation kinetics. Studies [89] on another phospholipid, dimyristoyl phosphatidyl ethanolamine (DMPE), similarly argue for the two-phase interpretation. The circular LC domains pack into what appears to be a hexagonal superlattice, but the characteristic length

varies continuously and uniformly with compression from one phase boundary to the other.

In contrast to these results, however, it has been [84] found that lamellar (labyrinth) and hexagonal phases exist in well-defined areas of the DPPC + cholesterol phase diagram and that it is possible to observe coexistence between these two modulated phases. Similarly, To *et al* [90] have observed a stable stripe pattern in the LE-G coexistence region of D-myristoylalanine, an enantiomeric fatty amino acid. The stripe spacing is uniquely defined by the relative amounts of the G and LE phases. The experimental situation is therefore ambiguous and it is useful, then, to examine theoretically the nature of possible modulated phases in monolayers.

12.3.3 Dipolar and Charged Langmuir Monolayers

For neutral amphiphiles, we consider for simplicity only the case where the average dipole moment points along the perpendicular $\vec{z}$-direction, $\mu_z \equiv \langle \mu \rangle$. A non-vanishing in-plane component of the dipole moment stabilizes elongated structures and has been investigated as well [52,76]. As is shown below, an in-plane density wave of the dipoles will reduce the overall long-range repulsive dipolar interaction. Let $\phi(\vec{\rho})$ denote the amphiphile density at position $\vec{\rho}$ in the surface. For an amphiphile density with wavevector $\vec{q}$, *i.e.*, $\phi(\vec{\rho}) = \phi_o + \phi_q \cos(\vec{q}\cdot\vec{\rho})$, this energy lowering is given by:

$$\Delta F_{\rm el} = -\frac{1}{2}\frac{\epsilon_0}{\epsilon(\epsilon+\epsilon_0)}|q|\mu_z^2\phi_q^2 \tag{12.9}$$

ϵ (ϵ_0) is the water (air) dielectric constant as shown in Fig. 12.7. In Eq. (12.9), the dipoles are assumed to be *totally* immersed in the water and the interaction is screened by approximately ϵ^2. However, since the polar moieties lie very close to the air-water interface, the *effective* dielectric constant, ϵ^*, felt by the dipoles is expected to be intermediate between the bulk water value, $\epsilon = 80$, and that of vacuum, $\epsilon_0 = 1$. In addition, if the aliphatic tail of the molecules also contributes to the molecular dipole

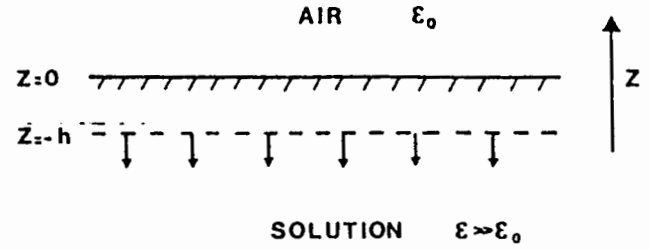

FIGURE 12.7. A flat interface at $z = 0$ separates air (dielectric constant ϵ_0) from an aqueous solution ($\epsilon \gg \epsilon_0$). Dipoles are confined to the plane $z = -h$ and the electrostatic energy is calculated in the limit $h \to 0$

moment, then some of the dipolar interactions are not screened. The linear dependence of ΔF_{el} in (12.9) on the modulation wavevector $|q|$ is a consequence of the long-range ($\sim 1/r^3$) character of the dipolar forces. In general, an algebraically decaying interaction, $F_{el} \sim 1/r^{d+\sigma}$, where d is the spatial dimension, will have a Fourier component with a $|q|^\sigma$ dependence. For dipoles, $d+\sigma = 3$, $d = 2$, hence, $\sigma = 1$.

If the amphiphiles are *charged* and an electrolyte is added to the water, the electric potential can be obtained from the Poisson-Boltzmann equation [78]. Here, we restrict ourselves to the linearized version of the Poisson-Boltzmann equation for the electrostatic potential V:

$$\begin{aligned} \nabla^2 V(\vec{r}) &= \kappa^2 V(\vec{r}) \quad \text{for} \quad z < 0 \\ \nabla^2 V(\vec{r}) &= 0 \qquad\quad \text{for} \quad z > 0 \end{aligned} \tag{12.10}$$

where κ^{-1} is the Debye-Hückel screening length. We solve the electrostatic problem (12.10) for a modulation in the surface charge density $\sigma(\vec{\rho}) = e\phi_0 + e\phi_q \cos(\vec{q}\cdot\vec{\rho})$, with the appropriate boundary conditions at $z = 0$.

The electrostatic energy is then given by

$$F_{el} = \frac{1}{2}\int \sigma(\vec{\rho})\, V(\vec{\rho}, z=0)\, d^2\vec{\rho} \quad = \quad \frac{e^2\phi_q^2}{2(\varepsilon\kappa_1 + \varepsilon_0|q|)} \tag{12.11}$$

where in (12.11) ${\kappa_1}^{-1}$ is the effective screening length for the q-mode, $\kappa_1^2 = \kappa^2 + q^2$, and we omit the average electrostatic contribution depending only on ϕ_0. For concentrated ionic solutions, the Debye-Hückel screening length is small: $\kappa >> q$. In this case, when (12.11) is expanded in powers of q/κ, equation (12.9) is recovered. The counter ions together with the surface charges form effective dipoles at the water surface with a dipole moment

$$\mu_z = \frac{e}{\kappa}\sqrt{1+\varepsilon_0/\varepsilon} \quad \simeq \quad e\kappa^{-1} \quad \text{for} \quad \varepsilon >> \varepsilon_0 \tag{12.12}$$

By changing the ionic strength in the solution, it is possible to reach $\kappa^{-1} \simeq 10\text{Å}$, corresponding to strong dipoles. In the opposite limit of dilute electrolytes, $q >> \kappa$, the electrostatic interactions are almost unscreened [91] and the interaction is Coulombic $\sim 1/r$.

As we shall see below, electrostatic interactions tend to stabilize phases with modulated density. Phase diagrams incorporating the possibility of modulated phases were calculated within the framework of the mean-field approximation in two cases: (*i*) close to a critical point where only the most dominant q-mode is considered, and (*ii*) at low-temperatures where entropy is neglected.

12.3.3.1 Landau theory close to a critical point

Close to the critical point, the free energy can be written phenomenologically [78-79] as a Landau expansion in the order parameter,

$$\psi(\vec{\rho}) = \phi(\vec{\rho}) - \phi_c \tag{12.13}$$

where ϕ_c is the amphiphile density at the critical temperature, T_c. The expansion contains only even terms in ψ

$$\Delta F_0/k_BT = \frac{1}{2}d(T - T_0)\psi^2(\vec{\rho}) + \frac{1}{4}u\psi^4(\vec{\rho}) \tag{12.14}$$

where the coefficients, $d > 0$ and $u > 0$, can be obtained from an expansion of the monolayer free-energy of mixing. Note that T_0 is the critical point *only* in the absence of the dipolar interactions. Since the electrostatic interactions favor spatial modulations, we also have to consider the energy gain and loss as an in-plane modulation of the two-dimensional concentration created. The *gain* will be in the electrostatic energy

$$F_{el}/k_BT = \frac{1}{2}\int \psi(\vec{\rho})g(\vec{\rho} - \vec{\rho}\,')\psi(\vec{\rho}\,')\,d^2\rho\,d^2\rho' \tag{12.15}$$

where $g(\rho) = k_BTb^3/2\pi\rho^3$ and $b^3 = \mu_z^2\epsilon_0/[\epsilon(\epsilon + \epsilon_0)k_BT]$.

The energy *loss* is the interfacial line energy between domains in a 2D geometry. For small density variations, the line energy is written to lowest order in a gradient expansion as:

$$F_I/k_BT = \frac{1}{2}a^{*2}\int(\nabla\psi)^2\,d^2\rho \tag{12.16}$$

with a^* being the minimum (compact) area per molecule. In Fourier space, eqs. (12.15) and (12.16) can be expressed as

$$(F_{el} + F_I)/k_BT = \frac{1}{2}\sum_q(a^{*2}q^2 - b^3|q|)\psi_q^2 \tag{12.17}$$

where $\psi(\vec{\rho}) = \psi_0 + \sum_q \psi_q \cos(\vec{q}\cdot\vec{\rho})$. The dominant q-mode is the one minimizing the ψ_q^2 coefficient in (12.17).

$$|\vec{q}\,|^* = b^3/2a^{*2} \tag{12.18}$$

Close to a critical point, it is a good approximation [85,92] to consider only modulations with magnitude q^* in addition to the homogeneous (q=0) solutions: $\psi(\vec{\rho}) = \psi_0$ and $\psi(\vec{\rho}) = -\psi_0$ for the condensed and dilute phases, respectively. Two types of spatial modulation of the two-dimensional density are considered [78,85]:

(i) a stripe-like phase, $\psi_S(\vec{\rho}) = \psi_0 + \psi_q \cos q^*x$. (See Fig. 12.8.)

(ii) a hexagonal phase, $\psi_H(\vec{\rho}) = \psi_0 + \sum_{i=1}^3 \psi_q \cos(\vec{k}_i\cdot\vec{\rho}_i)$, with $|\vec{k}_i| = q^*$ and $\sum_{i=1}^3 \vec{k}_i = 0$. (See Fig. 12.9.)

The phase diagram can be calculated by comparing the homogeneous free energy F_0 with the stripe and hexagonal ones, F_S and F_H, respectively.

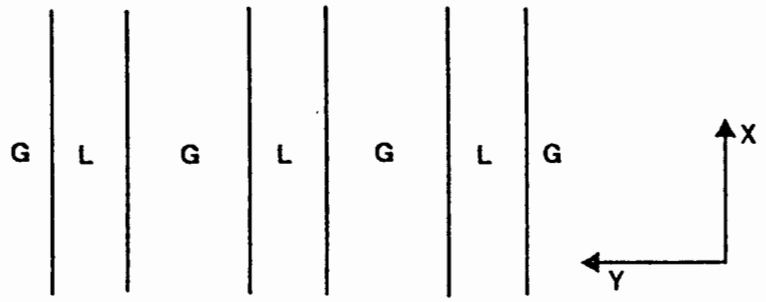

FIGURE 12.8. The stripe phase is shown schematically, where the stripes are chosen to be in the x direction. Domain walls (which are sharp only at low temperatures) separate denser liquid (L) from dilute gas (G). Close to the critical point, the density profile is sinusoidal and given by ψ_S in Sec. 12.3.3.1.

$$F_0 = \frac{\delta}{2}M_0^2 + \frac{1}{4}M_0^4 \tag{12.19}$$

$$F_S = F_0 + M_q^2(\delta - 1 + 3M_0^2) + \frac{3}{2}M_q^4 \tag{12.20}$$

$$F_H = F_0 + M_q^2(3\delta - 3 + 9M_0^2 + 12M_0M_q) + \frac{45}{2}M_q^4 \tag{12.21}$$

where,

$$\eta^2 = b^6/a^{*3} \quad , \quad \delta = 4d(T - T_0)/\eta^2$$
$$M_0^2 = (4u/\eta^2)\psi_0^2 \quad , \quad M_q^2 = (u/\eta^2)\psi_q^2 \tag{12.22}$$

In Fig. 12.10, the phase diagram in the reduced temperature, $\delta \sim T - T_0$, — reduced average concentration, $M_0 \sim \langle\phi\rangle - \phi_c$, plane is shown, whereas in Fig. 12.11, the same phase diagram is drawn in the chemical potential μ — reduced temperature δ plane. The chemical potential is the thermodynamical variable that is coupled to the average concentration M_0. The usual coexistence region between liquid and gas regions, $M_0^2 = \delta$, is largely modified. The critical point at $\delta_c = 0$ ($T_c = T_0$) is renormalized upwards to $\delta_c = 1$ ($T_c = T_0 + b^3/4da^{*3}$), and is the termination point of five distinct phases: gas (G), stripe (S), hexagonal (H), inverted hexagonal (IH), and liquid (L). The gas and liquid phases are isotropic dilute and dense phases, respectively. All the transition lines below the critical point ($M_0 = 0$, δ_c) are first-order. Consequently, there are four regions of two-phase coexistence between the phases. Although the single q-mode expansion is valid close to a critical point, it cannot be trusted for low temperatures. For example, this theory predicts a disappearance of the stripe and hexagonal phases for δ less than δ_c, as seen in Figs. 12.10 and 12.11. To overcome this difficulty we give in the next section a proof of the existence of modulated phases at low temperatures.

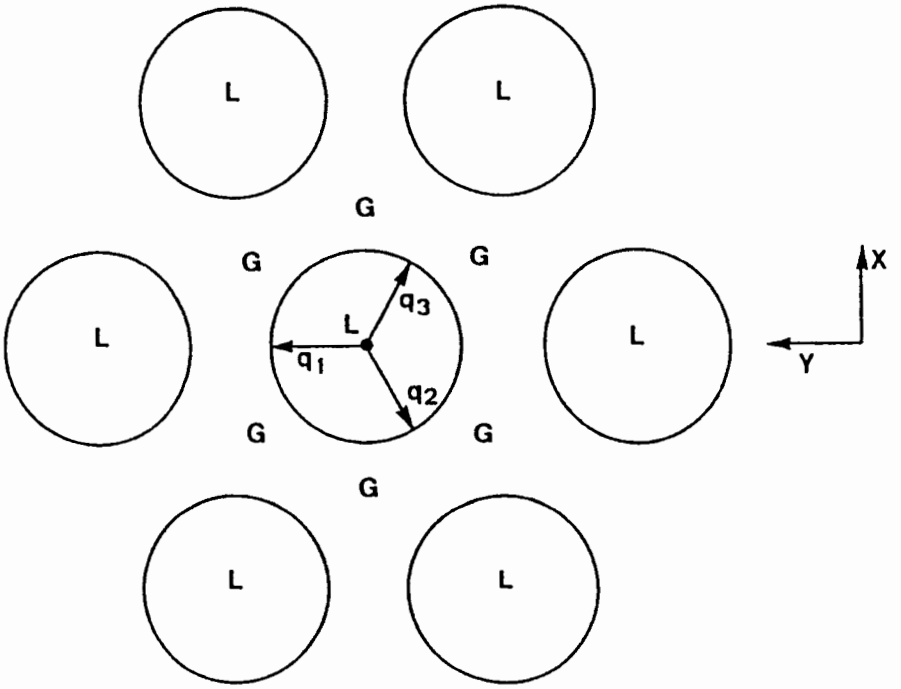

FIGURE 12.9. The hexagonal phase is shown schematically. Denser liquid "bubbles" (L) are separated via domain walls from a dilute gas background (G). Domain walls are sharp only at low temperatures. Close to T_c, the density profile is given by ψ_H in Sec. 12.3.3.1.

12.3.3.2 Modulated phases at low temperatures

At low temperatures (far from the critical point) it is natural to replace the Landau expansion by a direct calculation of the modulated phase free energy. Here we neglect contributions from the entropy of mixing and focus wholly on the electrostatic energy and line tension effects. We show that at low temperatures modulated phases are still expected to be stable over a range of concentrations. For simplicity, only the stripe phase with sharp domain walls is considered. The stripe phase is formed from a periodic arrangement of stripes of the dilute phase of size D_G and of the dense phase of size D_L. The electrostatic free energy of the stripe phase is

$$F_{el}/k_BT = \frac{b^3}{\pi\ell}[x\phi_L^2 + (1-x)\phi_G^2] - \frac{b^3}{\pi D}(\phi_L - \phi_G)^2 \log\left(\frac{D}{\ell}\frac{\sin\pi x}{\pi}\right) \quad (12.23)$$

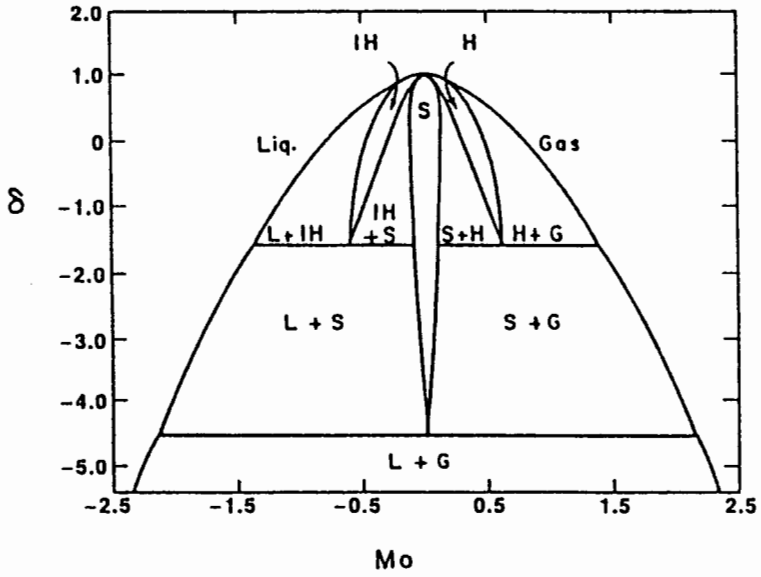

FIGURE 12.10. Phase diagram in the (M_0, δ) plane where $\delta \sim T - T_0$ is the reduced temperature and $M_0 \sim \langle\phi\rangle - \phi_c$ is the reduced concentration. The two isotropic phases, liquid (L) and gas (G), are separated by the hexagonal (H), stripe (S), and inverted hexagonal (IH) phases. Two-phases coexistence regions are also indicated. The phase diagram is obtained from Eqs. (12.19) – (12.22) and is valid only close to T_c.

where $x = D_L/D = D_L/(D_L + D_G)$ is the relative concentration of L and G, and $\ell \simeq \sqrt{a^*}$ is a microscopic cutoff. The first term represents the overall average contribution to the electrostatic energy and is independent of the periodicity D. The last term is an exact summation of the intra- and inter-stripe electrostatic interactions [93]. An additional contribution to the free energy difference ΔF between the stripe and the homogeneous phases with the same concentration comes from the line tension λ associated with every domain wall separating a G domain from an L one. The total free energy difference is thus

$$\Delta F = -\frac{k_B T b^3}{\pi D}(\phi_L - \phi_G)^2 \log\left(\frac{D}{\ell}\frac{\sin \pi x}{\pi}\right) + \frac{2\lambda}{D} \tag{12.24}$$

The equilibrium periodicity D^* of the stripe structure is given by minimizing (12.24) with respect to D, giving

$$D^* = \frac{\ell\pi}{\sin \pi x} \exp \beta \tag{12.25}$$

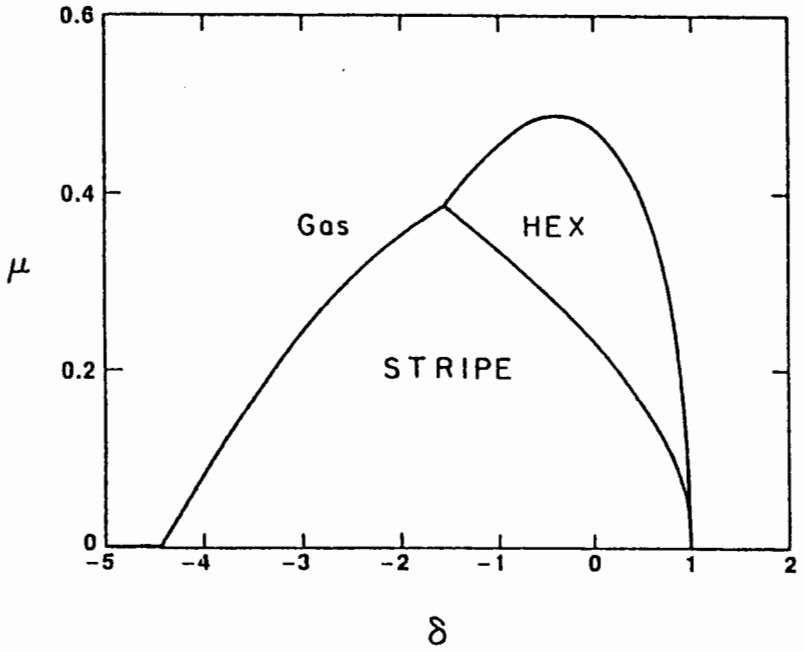

FIGURE 12.11. Phase diagram in the chemical potential μ - reduced temperature δ plane. The phase diagram is symmetric about $\mu = 0$ and is presented only for $\mu > 0$. First-order transition lines separate the isotropic dilute gas (G) from hexagonal (H) and stripe (S) phases. The phase diagram is obtained from Eqs. (12.19) - (12.22) and is valid only close to T_c.

where

$$\beta = \frac{2\pi\lambda}{k_B T b^3 (\phi_L - \phi_G)^2} + 1 \tag{12.26}$$

The exponential dependence of the periodicity D^* on the ratio between the line tension λ and the dipole interaction coefficient $b^3(\phi_L - \phi_G)^2 \sim \mu_z^2$ makes it difficult to give an *a priori* estimate of D^* since neither λ nor b are known accurately from experiments. In principle, b can be changed in a controlled way by tuning the electrolyte strength for a charged monolayer, allowing a check of Eq. (12.25). In addition, it has been found that cholesterol [74-77, 81-84] reduces the line tension, causing thinning of the domains in qualitative agreement with the theoretical prediction [78,94] of Eq. (12.25). Recently, direct measurements of the stripe periodicity with the surface fraction of G and LE phases in a single-component system and in the absence of line-active cholesterol [90] have been performed. The results are consistent with Eq. (12.25).

12.4 Dynamical Properties of Amphiphilic Monolayers

12.4.1 Lateral Diffusion in Monolayers

Since a monolayer of amphiphilic molecules spread at the water/air surface creates a 2D flat interface, it provides an example of a system undergoing a phase separation at zero gravity [95]. However, the dynamics of such a monolayer is not strictly two-dimensional since the motion of the amphiphilic molecules on the interface induces a *backflow* in the *water* subphase. This backflow, in turn, gives rise to hydrodynamic interactions between the amphiphilic molecules. Below we discuss the first stages of phase separation when viscous dissipation and electrostatic interactions are included in the analysis. It is important to note that since the dissipation takes place mostly in the water subphase due to the backflow effect, it has a three-dimensional character.

Imagine that we have a monolayer with an average surface concentration ϕ on the surface of a water subphase of thickness h. For simplicity, we assume that the water thickness h is smaller than the wavelength associated with concentration fluctuations of the monolayer. In this case, we can use the *lubrication approximation* [96] to describe the flow in the subphase, since the flow in the water is to a good approximation a local Poiseuille flow. A local fluctuation of the monolayer concentration, $\delta\phi(x)$, leads to a local modulation of the surface pressure $\Pi(x)$ and hence, modifies the surface tension, $\gamma(x) = \gamma_0 - \Pi(x)$ and produces a stress at the free boundary (water/air interface). For a thin water subphase, the flow is a simple shear flow as shown in Fig. 12.12a, *i.e.*, the x-component of the velocity increases with z according to

$$v_x(z) = v_S(1 + \frac{z}{h}) \tag{12.27}$$

where v_S is the velocity of the amphiphiles at the surface $z = 0$, and $z = -h$ is the position of the water/solid interface.

At the free surface, the viscous stress must balance the gradient of surface tension

$$\sigma_{xz} = \eta\frac{\partial v_x}{\partial z} = \eta\frac{v_S}{h} = \frac{\partial\gamma}{\partial x} = -\frac{\partial\Pi}{\partial x} \tag{12.28}$$

and the surface flow of the amphiphile is

$$\vec{J}_s = \phi\vec{v_S} = \phi(-\vec{\nabla}\Pi)\frac{h}{\eta} = -D_c\vec{\nabla}\phi \tag{12.29}$$

Equation (12.29) defines the cooperative diffusion coefficient of the amphiphiles, D_c

$$D_c = \phi\frac{h}{\eta}\frac{\partial\Pi}{\partial\phi} \tag{12.30}$$

which is concentration dependent.

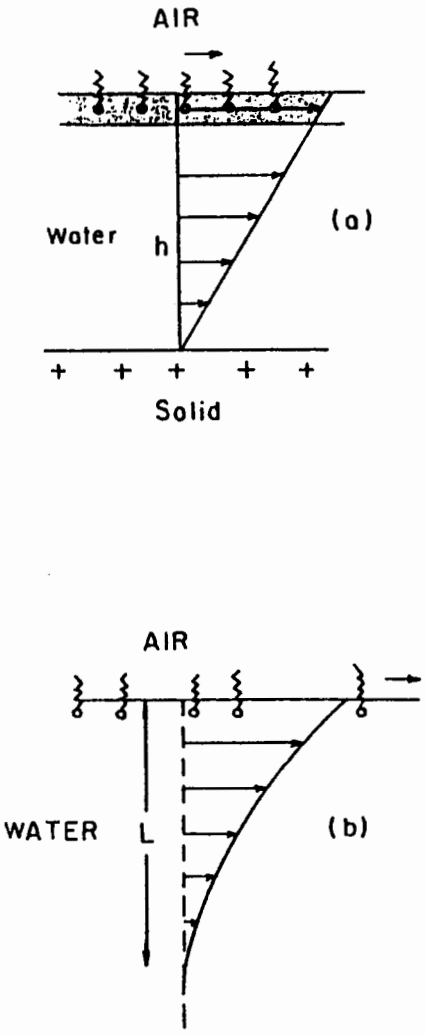

FIGURE 12.12. Backflow induced by motion in the monolayer: (a) for a thin liquid subphase of thickness h on a solid. The flow is a simple shear flow; (b) for a bulk liquid, the flow penetrates into the liquid with an exponential decay characterized by a small penetration length of thickness L.

The diffusion coefficient is calculated for two regimes:

The first is the very dilute regime corresponding to the gas state of the monolayer: the surface pressure obeys an ideal gas law, $\Pi = \phi k_B T$ and D_c is proportional to $\phi \sim 1/a$

$$D_c = \phi \frac{k_B T}{\eta} h = (\phi \ell h) D_0 \tag{12.31}$$

where $D_0 = k_B T/\eta\ell$ is the molecular diffusion constant and ℓ is a molecular length. Equation (12.31) describes the cooperative part of the diffusion. In principle, we should add a term of order D_0 due to the diffusion of single amphiphilic molecules in the absence of any neighbors. However, since $\phi\ell h > 1$ in all practical cases, $D_c \gg D_0$, and we neglect the molecular diffusion term.

We note that (12.31) represents a *"hypodiffusive"* case [97] since D_c vanishes in the limit of small surface concentration, $\phi \to 0$, and the spreading of amphiphilic molecules at the free surface is described by a nonlinear diffusion equation

$$\frac{\partial \phi}{\partial t} = D_c(\phi) \nabla^2 \phi \tag{12.32}$$

A sharp edge of the amphiphile concentration profile, $\phi(x)$, is expected [98] in this hypodiffusive case.

The second regime we consider is when the monolayer is in a liquid state in which case $\phi \partial \Pi/\partial\phi$ becomes of order $k_B T/\ell^2$. Equation (12.30) can then be written as

$$D_c = D_0 \frac{h}{\ell} \tag{12.33}$$

The diffusion coefficient D_c is extremely large; it is the product of the molecular diffusion D_0 and a factor h/ℓ, where h is a macroscopic length and ℓ is a molecular length.

In conclusion, backflow leads to a strong enhancement of the amphiphile diffusion coefficient for a shallow water subphase. For a bulk water subphase, the same conclusion holds but the flow penetrates only up to a layer of thickness L (from the surface), which is frequency dependent [96], as can be seen on Fig. 12.12b. For a mode of wavevector q and frequency ω one has

$$L^{-1} = \sqrt{q^2 + \omega\rho/\eta} \tag{12.34}$$

where η/ρ is the kinematic viscosity . For q vectors larger than $q_c \simeq \omega\rho/\eta$, inertial effects are negligible: $L^{-1} \simeq q$ and $D_c(q)$ is then given by

$$D_c(q) = \frac{D_0}{q\ell} \tag{12.35}$$

12.4.2 Dynamics of Phase Separation in Monolayers

Now imagine a rapid change in either temperature or surface pressure such that the monolayer is rapidly quenched from a homogeneous one-phase region into a two-phase coexistence region or into a one-phase modulated region. If in the final state the original homogeneous phase is *metastable*, the initial stages of the growth dynamics are characterized by a nucleation process requiring an activation energy to initiate the phase separation. On the other hand, if the original homogeneous phase is *unstable* after the quench, the initial stage of the dynamics is characterized by a fast amplification of local concentration fluctuations [99-100]. For the monolayer geometry this amplification causes a divergence in the so-called longitudinal Lucassen modes [101-102]. This dynamical process is at the basis of *spinodal decomposition* and we will consider it now in the specific case of dipolar monolayers with electrostatic interactions.

The longitudinal modes of a monolayer on a bulk liquid have been studied in detail by Lucassen [101]. Contrary to usual liquid – liquid phase separation where the soft mode is diffusive, they are propagative in the range of small wavevectors because the inertial component is important. For simplicity, we discuss here [103] only the case of an amphiphilic monolayer covering a thin liquid subphase. As in the previous section, the hydrodynamics is treated only within the lubrication approximation which simplifies the dispersion relation.

When the monolayer in a homogeneous state is suddenly quenched into the coexistence region, it behaves as an elastic membrane with $u_q = u_0 e^{iqx} e^{i\omega t}$ being its displacement in the x-direction for a wavevector q. The fluctuation of the surface density ψ_q is related to u_q by a conservation equation $\psi_q = -\partial u_q/\partial x$. For any concentration fluctuation, there is an elastic restoring force f_{elastic}, which can be calculated from the free energy density (12.14-16)

$$(\Delta F_0 + F_{\text{el}} + F_I)/k_B T = \frac{1}{2} d(T - T_0)\psi^2(\vec{\rho}) + \frac{1}{4} u\psi^4(\vec{\rho}) + \frac{1}{2}\sum_q (a^{*2}q^2 - b^3|q|)\psi_q^2 \qquad (12.36)$$

where the order parameter ψ and the coefficients d and u were introduced in Sec. 12.3. The optimal mode that minimizes (12.36) is $|\vec{q}\,|^* = b^3/2a^{*2}$ [see Eq. (12.18)] and the critical temperature is renormalized upwards: $T_c = T_0 + b^6/4da^{*2}$. The elastic restoring force f_{elastic} calculated from (12.36) is

$$f_{\text{elastic}}(q) = E(q)\frac{\partial^2 u_q}{\partial x^2} \qquad (12.37)$$

with

$$E(q)/k_B T = d(T - T_0) + a^{*2}q^2 - b^3|q| \qquad (12.38)$$

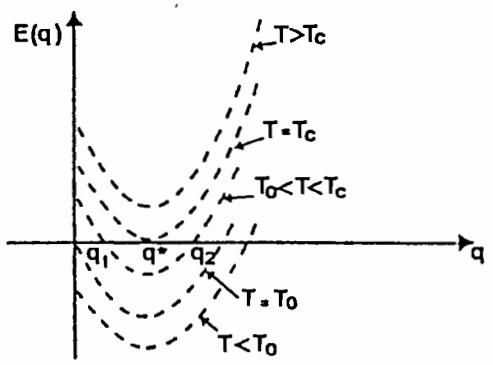

FIGURE 12.13. Elastic modulus E of a polar Langmuir monolayer as a function of the wavevector q for several temperatures. Due to the repulsive long-range dipolar interactions, the sign of E is reversed at a finite $q = q^*$ corresponding to the periodicity of the modulated phase, $2\pi/q^*$.

The membrane is unstable if the elastic restoring force is negative and $E(q) = 0$ defines the spinodal line. The dependence of $E(q)$ on q is shown in Fig. 12.13 for several temperatures. For $T > T_c$, E is always positive, *i.e.*, there is no instability, whereas for $T = T_c$, the first unstable mode occurs at $q = q^*$. For $T < T_c$, the range of the unstable modes is $q_{\min} < q^* < q_{\max}$, and for even lower temperatures, $T < T_0$, the unstable q-modes start from $q_{\min} = 0$ and terminate at $q_{\max}$.

For a monolayer covering a thin water layer of thickness h and in the limit $qh \ll 1$, the lubrication approximation holds and any fluctuation in the monolayer induces a shear flow in the liquid. The viscous force on the monolayer is thus simply given by

$$f_{\text{visc}} = \frac{\eta}{h}\frac{\partial u_q}{\partial t} \tag{12.39}$$

where η is the water viscosity.

The balance between f_{elastic} (12.37) and f_{visc} (12.39) determines the equation of motion:

$$E(q)\frac{\partial^2 u_q}{\partial x^2} = \frac{\eta}{h}\frac{\partial u_q}{\partial t} \tag{12.40}$$

This leads to a diffusive mode

$$\frac{1}{\tau_q} = D_c q^2, \quad \text{with} \qquad D_c = E\frac{h}{\eta} \tag{12.41}$$

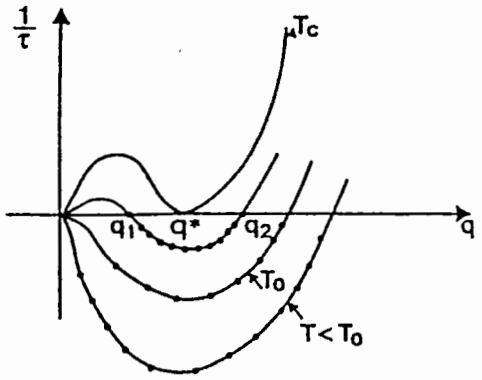

FIGURE 12.14. Relaxation time τ_q of the longitudinal mode of a planar Langmuir monolayer deposited on a thin liquid film. The first instability ($\tau_q^{-1} < 0$) occurs at the same q-vector that determines the modulations periodicity.

For $E < 0$, $D_c < 0$ and the fluctuations are amplified. If $T \leq T_c$, the amplified modes are the ones close to q^*, and in the range $q_{\min} < q < q_{\max}$, as shown in Fig. 12.14. As T decreases, the lower threshold of the instability, $q_{\min}$, goes to zero and the maximal wavevector $q_{\max}$ increases. $q_{\max}$ varies from being equal to q^* at T_c to a large value at low temperatures, $q_{\max}^2 = d(T_0 - T)a^{*2}$. Note that in this limit $q_{\max}$ is independent of the dipole-dipole interactions.

The results described above can be extended to the case of a monolayer on a thick (bulk) water subphase. For a shallow quench to temperatures just below T_c, the characteristic time is still given by Eq. (12.41), with $h = q^{-1}$ and $D_c = E/q\eta$. For a deep temperature quench below T_c, $T \ll T_c$, the modes are propagative and the dipolar interactions are negligible.

12.5 Conclusions and Future Prospects

The growing body of experimental research on monolayers has resolved many long-standing controversies about the nature of monolayer phases but at the same time has posed many new questions. The nature of the transitions G → LE → LC has been clarified by experiments and much theoretical effort has gone into understanding the sequence of phases as a dilute monolayer is compressed. But the more recent experiments, which have confirmed the existence of many condensed phases, have in essence turned the problem about — how does one understand the sequence of phases that arise when a close-packed monolayer is expanded?

In part, the answer to this question can be found in theories that have been applied to liquid crystals, but the analogies between monolayers and smectics are not exact. The water surface and the bifunctional nature of the amphiphile break the symmetry and lead to new phenomena. In monolayers there is an intriguing coupling between microscopic properties — such as molecular structure, electrostatic interactions, and chirality — and the mesoscopic and macroscopic scales. The ease with which the density of a monolayer can be changed allows a multiplicity of phases to be explored for a single amphiphile and therefore makes it possible to examine in a systematic way how subtle changes in molecular interactions affect the phase behavior.

The line tension between monolayer phases is a key parameter in the theories discussed in this chapter. Measurements of the line tension at the LE-LC and the LE-G interfaces have very recently been undertaken, but the results are rather imprecise. Even less well determined is the anisotropy in the line tension, which manifests itself in the equilibrium shapes of domains and the formation of dendrites.

There is much to be learned about dynamic processes in monolayers. With the exception of studies of the evolution of monolayer foams, nothing is known about the kinetics of phase transitions and growth. While there have been light scattering from surface waves and classical viscometry measurements on monolayer systems, relatively little is known about transport processes in the films.

The interplay between the polar heads of the monolayer and solutes in the subphase is beginning to be examined. It is well known, for example, that divalent ions can induce profound changes in the molecular arrangement within the monolayer. Conversely, an ordered monolayer can be used as a convenient template to induce ordering of a layer of ions or molecules adsorbed from the subphase. This may lead the way to two-dimensional crystallization of low-molecular-weight compounds or even of proteins.

Another challenging future direction is to investigate the effect of mixing in Langmuir monolayers. For example: monolayers composed of two different amphiphiles, two surfactants or, even more generally, mixed monolayers of amphiphiles and polymers, or amphiphiles and proteins. The structure and phase behavior of the mixed monolayer depend both on the overall density (which can be controlled by the surface pressure) and the relative concentration of the two species. As in the case of DPPC + cholesterol, superstructures and spatial inhomogeneities can be strongly coupled to the relative composition.

Apart from their academic interest, mixed monolayers may have many practical applications. It may be possible, for example, to achieve nanolithography and further decrease the dimensions of electonic components by embedding proteins in a Langmuir monolayer and then transferring the monolayer to a solid support. The proteins can then be removed to

create holes of few tens of Angstroms in diameter. It may also be possible to create ultra-thin membranes for use in separation processes by mixing a polymerizable amphiphile with another non-reactive component. Once crosslinking has been achieved, the unreacted species can be removed and one is left with a two-dimensional mono-molecular membrane of controlled pore size.

To conclude, Langmuir monolayers are easily accessible and highly versatile two-dimensional systems. They also represent the simplest examples of self assemblying systems and can be viewed as model systems for biological cell membranes, vesicles, etc. Much remains to be done, but the activity in the field of monolayer research remains high and the prognosis for major advances is excellent.

Acknowledgements

A part of the theoretical results presented here have been obtained in collaboration with P. G. de Gennes and J. F. Joanny. This chapter was written while one of us (DA) was a Rothschild fellow at the Institut Curie, Paris. He would also like to acknowledge support from the U.S.-Israel Binational Science Foundation under grant No. 87-00338, and the Israel Academy of Sciences and Humanities. CMK acknowledges the support of the U.S. National Science Foundation under Grant CHE-9040092.

References

1. G. L. Gaines, Jr., *Insoluble Monolayers at Liquid-Gas Interfaces* (Interscience, New York, 1966); a) I. Langmuir, J. Am. Chem. Soc. **39**, 354 (1917); b) I. Langmuir, J. Chem. Phys. **1**, 756 (1933).
2. A. W. Adamson, *Physical Chemistry of Surfaces*, 4th Ed. (Wiley, New York, 1982), Chap. IV.
3. S. Ställberg-Stenhagen and E. Stenhagen, Nature **156**, 239 (1945).
4. E. Stenhagen in *Determination of Organic Structures by Physical Methods*,W. A. Braude and F. C. Nachod, eds. (Academic Press, New York, 1955).
5. M. Lundquist, Chem. Scr. **1**, 5 (1971).
6. M. Lundquist, Chem. Scr. **1**, 197 (1971).
7. C. M. Knobler, Adv. Chem. Phys. **77**, 397 (1990).
8. H. Möhwald, Ann. Rev. Phys. Chem. **41**, 441 (1990).
9. R. Peters and K. Beck, Proc. Natl. Acad. Sci. USA **80**, 7183 (1983).
10. V. von Tscharner and H. M. McConnell, Biophys. J. **36**, 409 (1981).
11. M. Lösche and H. Möhwald, Rev. Sci. Instrum. **55**, 1968 (1984).
12. B. G. Moore, C. M. Knobler, S. Akamatsu, and F. Rondelez, J. Phys. Chem. **94**, 4588, (1990).
13. V. T. Moy, D. J. Keller, H. E. Gaub, and H. M. McConnell, J. Phys. Chem. **90**, 3198 (1986).
14. X. Qui, J. Ruiz-Garcia, K. J. Stine, C. M. Knobler and J. V. Selinger, Phys. Rev. Lett. **67**, 703 (1991).
15. K. Kjaer, J. Als-Nielsen, S. A. Helm, P. Tippmann-Krayer and H. Möhwald, Thin Solid Films **159**, 17 (1988).
16. M. J. Grundy, R. M. Richardson, S. J. Roser, J. Penfold and R. C. Ward, Thin Solid Films **159**, 43 (1988).
17. One must be aware, however, that substitution of D for H in either the amphiphile or subphase may cause gross changes in the phase behavior. See, e.g., O. Bouloussa and M. Dupeyrat, Biochem. Biophys. Acta **896**, 239 (1987) and D. Vaknin, K. Kjaer, J. Als-Nielsen, and M. Lösche, Biophys. J. **59**, 1324 (1991).
18. H. Möhwald, Thin Solid Films **159**, 1 (1988).

19. S. Barton, A. Goudot, O. Bouloussa, F. Rondelez, B. Lin, F. Novak, A. Acero and S.A. Rice, J. Chem. Phys. 96, 1343 (1992).

20. T. Rasing, Y. R. Shen, M. W. Kim, and S. Grubb, Phys. Rev. Lett. 55, 2903 (1985).

21. X. Zhao, C. Goh, and K. B. Eisenthal, J. Phys. Chem. 94, 2222 (1990).

22. P. Guyot-Sionnest, J. H. Hunt, and Y. R. Shen, Phys. Rev. Lett. 59, 1597 (1987).

23. R. A. Dluhy, J. Phys. Chem. 90, 1373 (1986).

24. S. Garoff, H. W. Deckman, J. H. Dunsmuir, M. S. Alvarez and J. M. Bloch, J.de Physique 49, 701 (1986).

25. A. Fischer, M. Lösche, M. Möhwald and E. Sackmann, J. de Physique Lett. 45, L-785 (1984).

26. J. K. H. Hörber, C. A. Lang, T. W. Hänsch, W. M. Heckl and H. Möhwald, Chem. Phys. Lett. 145, 151 (1988).

27. E. Meyer, L. Howald, R. M. Overney, H. Heinzelmann, J. Frommer, H.-J. Güntherodt, T. Wagner, H. Schier, and S. Roth, Nature 349, 398 (1991).

28. G. S. Patil, S. S. Katti, and A. B. Biswas, J. Colloid Interface Sci. 25, 462 (1967).

29. B. M. Abraham, K. Miyano, J. B. Ketterson, and W. Q. Xu, Phys. Rev. Lett. 51, 1975 (1983).

30. P. J. Winch and J. C. Earnshaw, J. Phys.: Condens. Matter 1, 7187 (1989).

31. Th. Rasing, H. Hsiung, Y. R. Shen, and M. W. Kim, Phys. Rev. A 37, 2732 (1988).

32. S. Hénon and J. Meunier, Rev. Sci. Instrum. 62, 936 (1991).

33. D. Hönig and D. Möbius, J. Phys. Chem. 91, 4590 (1991).

34. S. Akamatsu and F. Rondelez, J. de Physique 1, 1309 (1991).

35. M. W. Kim and D. S. Cannell, Phys. Rev. A 13, 411 (1976).

36. N. R. Pallas and B. A. Pethica, J. Chem. Soc. Faraday Trans. I 83, 585 (1987).

37. A detailed discussion of this problem can be found in Ref. 7.

38. N. R. Pallas and B. A. Pethica, Langmuir **1**, 509 (1985).

39. J. C. Earnshaw and P. J. Winch, J. Phys. : Condens. Matter **2**, 8499 (1990).

40. A. M. Bibo and I. R. Peterson, Adv. Mater. **2**, 151 (1990).

41. K. Kjaer, J. Als-Nielsen, C. A. Helm, L. A. Laxhuber and H. Möhwald, Phys. Rev. Lett. **58**, 2224 (1987).

42. C. A. Helm, H. Möhwald, K. Kjaer and J. Als-Nielsen, Europhys. Lett. **4**, 697 (1987).

43. H. Möhwald, R. M. Kenn, D. Degenhardt. K. Kjaer and J. Als-Nielsen, Physica A **168**, 127 (1991).

44. B. Lin, M. C. Shih, T. M. Bohanon, G. E. Ice and P. Dutta, Phys. Rev. Lett. **65**, 191 (1990).

45. K. Kjaer, J. Als-Nielsen, C. A. Helm, P. Tippmann-Krayer and H. Möhwald, J. Phys. Chem. **93**, 3200 (1989).

46. R. M. Kenn, C. Böhm, A. M. Bibo, I. R. Peterson, H. Möhwald, J. Als-Nielsen and K. Kjaer, J. Phys. Chem. **95**, 2092 (1991).

47. M. L. Schlossman, D. K. Schwartz, P. S. Pershan, E. H. Kawamoto, G. J. Kellog and S. Lee, Phys. Rev. Lett. **66**, 1599 (1991).

48. S. W. Barton, B. N. Thomas, E. B. Flom, S. A. Rice, B. Lin, J. B. Peng, J. B. Ketterson and P. Dutta, J. Chem. Phys. **89**, 5898 (1988).

49. B. Lin, J. B. Peng, J. B. Ketterson, P. Dutta, B. N. Thomas, J. Buontempo and S. A. Rice, J. Chem. Phys. **90**, 2393 (1989).

50. C. M. Knobler, Science **249**, 870 (1990).

51. H. Bercegol, F. Gallet, D. Langevin and J. Meunier, J. de Physique **50**, 2277 (1989).

52. P. Muller and F. Gallet, Phys. Rev. Lett. **67**, 1106 (1991); P. Muller and F. Gallet, J. Phys. Chem. **95**, 3257 (1991).

53. M. L. Mitchell and R. A. Dluhy, J. Am. Chem. Soc. **210**, 712 (1988).

54. A. Fisher and E. Sackmann, J. de Physique **45**, 517 (1984).

55. A. M. Bibo, C. M. Knobler and I. R. Peterson, J. Phys. Chem. **95**, 5591 (1991)

56. S. B. Dierker, R. Pindak, and R. B. Meyer, Phys. Rev. Lett. **56**, 1819 (1986).

57. L. Onsager, Ann. N. Y. Acad. Sci. **51**, 625 (1949).

58. See, for example, M. A. Cotter, J. Chem. Phys. **66**, 4710 (1977).

59. A. Halperin, I. Schechter and S. Alexander, J. Chem. Phys. **86**, 6550 (1987).

60. Z.-Y. Chen, J. Talbot, W. M. Gelbart and A. Ben-Shaul, Phys. Rev. Lett. **61**, 1376 (1988).

61. D. Kramer, A. Ben-Shaul, Z.-Y. Chen and W. M. Gelbart, J. Chem. Phys. **96**, 2236 (1992).

62. C. M. Roland, M. J. Zuckermann and A. Georgallas, J. Chem. Phys. **86**, 5812 (1987).

63. A. Caille, D. Pink, F. de Verteuil and M. J. Zuckermann, Can. J. Phys. **58**, 581 (1980).

64. J. L. Viovy, W. M. Gelbart and A. Ben-Shaul, J. Chem. Phys. **87**, 4114 (1987).

65. See, for example, discussion in the review by G. M. Bell, L. L. Combs and L. J. Dunne, Chem. Rev. **81**, 15 (1981).

66. S. Shin, Z.-G. Wang and S. A. Rice, J. Chem. Phys. **92**, 1427 (1990).

67. P. J. Flory, *Principles of Polymer Chemistry* (Cornell, 1953).

68. T. L. Hill, *Introduction to Statistical Thermodynamics* (Addison-Wesley, 1960).

69. R. S. Cantor and P. M. McIlroy, J. Chem. Phys. **90**, 4423 and 4431 (1989).

70. K. To, A. Goudot, O. Bouloussa and F. Rondelez, unpublished.

71. J. Harris and S. A. Rice, J. Chem. Phys. **89**, 5898 (1988).

72. J. P. Bareman, G. Cordini and M. L. Klein, Phys. Rev. Lett. **60**, 2152 (1988).

73. See, for example, K. A. Motakabbir and M. Berkowitz, Chem. Phys. Lett. **176**, 61 (1991); M. Townsend, J. Gryko and S. A. Rice, J. Chem. Phys. **82**, 4391 (1985).

74. H. M. McConnell and V. T. Moy, J. Phys. Chem. **92**, 4520 (1988).

75. A. Miller and H. Möhwald, J. Chem. Phys. **86**, 4258 (1987).

76. H. M. McConnell, Ann. Rev. Phys. Chem. **42**, 171 (1991); J. Phys. Chem. **42**, 17, (1991).

77. T. K. Vanderlick and H. Möhwald, J. Phys. Chem. 94, 886 (1990).

78. D. Andelman, F. Brochard and J. F. Joanny, J. Chem. Phys. 86, 3673 (1987).

79. D. Andelman, F. Brochard, P. G. de Gennes and J. F. Joanny, C. R. Acad. Sci. (Paris) **301**, 675 (1985).

80. D. Andelman, Mat. Res. Soc. Symp. Proc. **177**, 337 (1990).

81. A. Miller and H. Möhwald, Europhys. Lett. **2**, 67 (1986).

82. M. Flörsheimer and H. J. Möhwald, Chem. Phys. Lipids **49**, 231 (1989).

83. S. Subramaniam and H. M. McConnell, J. Phys. Chem. **91**, 1715 (1987).

84. M. Seul and M. J. Sammon, Phys. Rev. Lett. **64**, 1903 (1991).

85. T. Garel and S. Doniach, Phys. Rev. B **26**, 325 (1982).

86. C. Kooy and U. Enz, Phillips Res. Rep. **15**, 7 (1960); M. Seul, unpublished.

87. R. E. Rosensweig, *Ferrohydrodynamics* (Cambridge, 1985).

88. C. A. Helm and H. Möhwald, J. Phys Chem. **92**, 1261 (1988).

89. M. Lösche, H.-P. Duwe and H. Möhwald, J. Colloid Interface Sci. **126**, 432 (1988).

90. K. To, S. Akamatsu and F. Rondelez, unpublished.

91. P. Pieranski, Phys. Rev. Lett. **45**, 569 (1980).

92. S. A. Brazovskii, Zh. Eksp. Teor. Fiz. **68**, 175 (1975) Sov. Phys. JETP **41**, 85 (1975)].

93. The exact summation of the inter-stripe electrostatic interactions is performed in Ref. 94 and is shown also in Ref. 80. In Ref. 78, the identical inter-stripe contribution is expressed as an infinite sum. Taking only the first few terms in the infinite sum gives qualitatively similar results.

94. D. J. Keller, H. M. McConnell and V. T. Moy, J. Phys. Chem. **90**, 2311 (1986).

95. P. G. de Gennes, C. R. Acad. Sci. (Paris) **290**, 119 (1980).

96. V. G. Levich, *Physicochemical Hydrodynamics* (Prentice Hall, New York, 1962).

97. P. G. de Gennes, in *Physics of Disordered Materials*, D. Adler, H. Fritzsche, and S. R. Ovshinsky, eds. (Plenum, New York, 1985), p. 227.

98. J. Crank, *The Mathematics of Diffusion* (Clarendon Press, Oxford, 1975).

99. J. D. Gunton, J. M. San Miguel and P. S. Sahni, in *Phase Transitions and Critical Phenomena*, Vol 8, C. Domb and J. Lebowitz, eds. (Academic Press, New York, 1983).

100. J. D. Gunton and M. Droz, *Introduction to the Theory of Metastable and Unstable States* (Springer, Heidelberg, 1983).

101. J. Lucassen, Trans. Faraday Soc. 64, 2221 (1968).

102. L. Kramer, J. Chem. Phys. 55, 2097 (1971).

103. F. Brochard, J. F. Joanny, D. Andelman, in *Physics of Amphiphilic Layers*, J. Meunier, D. Langevin and N. Boccara, eds. (Springer, Heidelberg, 1987).